# LATEX BASED MEMBRANE FOR OILY WASTEWATER FILTRATION: EFFECT OF DEGASSING

**DING SHI JIE**

**UNIVERSITI TUNKU ABDUL RAHMAN**

# LATEX BASED MEMBRANE FOR OILY WASTEWATER FILTRATION: EFFECT OF DEGASSING

**DING SHI JIE**

**A project report submitted in partial fulfilment of the requirements for the award of Bachelor of Engineering (Hons.) Petrochemical Engineering**

**Faculty of Engineering and Green Technology**
**Universiti Tunku Abdul Rahman**

**APRIL 2019**

# DECLARATION

I hereby declare that this project report is based on my original work except for citations and quotations which have been duly acknowledged. I also declare that it has not been previously and concurrently submitted for any other degree or award at UTAR or other institutions.

Signature : _____

Name : _____

ID No. : _____

Date : _____

## APPROVAL FOR SUBMISSION

I certify that this project report entitled "LATEX BASED MEMBRANE FOR OILY WASTEWATER FILTRATION: EFFECT OF DEGASSING" was prepared by DING SHI JIE has met the required standard for submission in partial fulfilment of the requirements for the award of Bachelor of Engineering (Hons.) Petrochemical Engineering in Universiti Tunku Abdul Rahman.

Approved by,

Signature : _____

Supervisor : _____

Date : _____

## ACKNOWLEDGEMENTS

I would like to thank everyone who had contributed to the successful completion of this project. I would like to express my gratitude to my research supervisor, Assoc. Prof. Dr. Yamuna a/p Munusamy for her invaluable advice, guidance and her enormous patience throughout the development of this research.

In addition, I would also like to express my gratitude to my loving parents and friends who had helped and given me encouragement.

# LATEX BASED MEMBRANE FOR OILY WASTEWATER FILTRATION: EFFECT OF DEGASSING

## ABSTRACT

Graphene oxide (GO) reinforced nitrile butadiene rubber (NBR) membrane was proven to be a promising candidate for oily wastewater treatment in this research. Two samples of latex with the same formulation were prepared via latex compounding and curing method. GO was prepared via exfoliation ahead of latex mixing so as to ensure uniform dispersion in NBR matrix. Fourier-Transform Infrared Spectroscopy (FTIR) and X-Ray Diffraction (XRD) were adopted to justify the conversion from graphene nanofiber (GNF) to graphite oxide (GtO).

Entrapped air was removed from one of the latex samples via vacuum suction. Thus, the degassing effect on membrane performances was investigated. Scanning Electron Microscopy (SEM) and Atomic Force Microscopy (AFM) were used to analyse the surface morphologies of the degassed and gassed membranes. SEM revealed the surface features, whereas AFM revealed the surface roughness. By visual inspection of the SEM micrographs, the degassed membrane possessed large pore size while the gassed membrane possessed uniform and small pore size. Both membranes exhibited folded structure but the degassed membrane had a rougher surface.

Tensile test was conducted to evaluate the mechanical properties of the membranes. The gassed membrane provided superior E-Modulus and ultimate tensile strength (UTS) of 2.034 and 22.31 MPa, respectively. However, the elongation at break was only 800%. A dead-end membrane test rig was adopted to simulate membrane filtration. When the membranes were subjected to synthetic oily wastewaters of 500 and 1000 ppm diesel oil content, the gassed membrane performed better in terms of oil rejection whereby oil rejection efficiencies above 90% at all

pressures and oil concentrations were achieved. Even though the degassed membrane could achieve higher fluxes, its inferior oil rejection efficiency was fatal in practise. The membrane filtration results are in agreement with the surface morphology of the degassed membrane because large pore size allowed oil and water droplets to pass through easily. The permeation flux of the gassed membrane which was 1300 $L/m^2 \cdot hr$ at 0.5 bar was already promising enough because it exceeded most polymeric membranes performances reported in literature.

**Keywords:** Graphene oxide; Nitrile butadiene rubber; Nanocomposite membrane; Degassing effect; Surface morphology; Tensile properties; Permeation flux; Oil rejection efficiency

# TABLE OF CONTENTS

# LIST OF TABLES

# LIST OF FIGURES

## LIST OF SYMBOLS / ABBREVIATIONS

| | |
|---|---|
| $W_{wet}$ | weight of wet sample, g |
| $W_{crucible}$ | weight of crucible, g |
| $W_{final}$ | constant weight after several times of drying, g |
| d | interlayer spacing, Å |
| λ | wavelength, nm |
| θ | maximum diffraction angle, ° |
| $J_p$ | permeation flux, $L/m^2 \cdot hr$ |
| $V_p$ | permeate Volume collected, mL |
| A | effective membrane area, $m^2$ |
| t | time taken to collect the measured volume of permeate, hr |
| R | oil rejection efficiency, % |
| $COD_p$ | COD level in the permeate, mg/L |
| $COD_f$ | COD level in wastewater feed, mg/L |
| $R_a$ | average roughness, nm |
| $R_q$ | root-mean-square roughness, nm |
| $R_{pv}$ | peak-to-valley roughness, nm |

| | |
|---|---|
| AFM | atomic force miscroscopy |
| BTEX | benzene, toluene, ethylbenzene, xylene |
| BOD | biochemical oxygen demand |
| BAF | biological aerated filter |
| COD | chemical oxygen demand |
| CFV | cross-flow velocity |
| DI | deionised |
| DAF | dissolved-air flotation |
| FESEM | field-emission scanning electron microscopy |

| | |
|---|---|
| FTIR | fourier-transform infrared |
| GO | graphene oxide |
| GtO | graphite oxide |
| GNF | graphene nanofiber |
| HRT | hydraulic retention time |
| IBAF | immobilised biological aerated filter |
| MF | microfiltration |
| MLSS | mixed liquor suspended solids |
| NF | nanofiltration |
| NBR | nitrile butadiene rubber |
| POME | palm oil mill effluent |
| PRE | petroleum refinery effluent |
| PAC | poly-aluminium chloride |
| PES | poly-ether sulfone |
| PSF | polysulfone |
| PVA | polyvinyl alcohol |
| PDVF | polyvinylidene fluoride |
| PZSS | poly-zinc silicate |
| RO | reverse osmosis |
| SEM | scanning electron microscopy |
| SDS | sodium dodecyl sulphate |
| SFR | steady fouling resistance |
| SPF | steady permeation flux |
| TDS | total dissolved solids |
| TKH | total Kjeldahl nitrogen |
| TOG | total oil and grease |
| TOC | total organic carbon |
| TSC | total solid content |
| TSS | total suspended solids |
| TMP | transmembrane pressure |
| UTS | ultimate tensile strength |
| UF | ultrafiltration |
| UASB | upflow anaerobic sludge blanket |

| | |
|---|---|
| XRD | X-ray diffraction |
| ZEDC | zinc diethyl dithiocarbamate |
| ZMBT | zinc mercaptobenzothiazole |

# CHAPTER 1

# INTRODUCTION

## 1.1 Background of Study

The issue of industrial pollution starts to take on more significance as a result of the rapid growth of Malaysia's industrial sector. Liquid wastes from industries, as well as solid wastes and air emissions, have become the prevailing concerns as they are the major pollution contributors which can adversely affect the environment. The water and wastewater treatment market in Malaysia is thereby driven by the municipal need for providing water and sanitary services. The main focus of the industrial water market falls on the food and beverage, petroleum refining, petrochemical and palm oil industries (International Trade Administration, 2016). Especially for the palm oil industry, Malaysia shares 39% of global palm oil production and 44% of global exports as reported by Malaysia Palm Oil Council (2012). As one of the world's leading producers and exporters of palm oil and its derivatives, Malaysia can never neglect the fact that oily wastewater treatment has correspondingly become more demanding.

Wastewater acts as a medium to transport unwanted materials removed from commercial and industrial establishments. Oils, fats, waxes and other related constituents that characterise oily wastewater are commonly termed oil and grease (Caltest Analytical Laboratory, 2014). These constituents exist in the form of oil-in-water emulsions. Before the water can be reused or discharged, the oil and grease contents of a wastewater must be removed so as to prevent posing any significant threats to the environment and human beings.

According to Tchobanoglous et al. (2014), grease can interfere with the biological life on the water surface by forming unsightly films. Thus, aquatic resources will be endangered if it is released into any watercourse. Apart from that, oil and grease derived from meats, cereals, seeds, nuts and palm fruits can hardly be degraded by microbes due to their low solubility in water. Fatty acids and glycerine are formed upon the reaction between mineral acids and oils in wastewater. When they are subjected to an alkaline condition, the glycerine will be further liberated and generate alkali salts of the fatty acids. These alkali salts, which are originally soluble in water, will become insoluble magnesium and calcium salts of the fatty acids in the presence of natural hardness constituents. These insoluble salts will be precipitated and eventually clog plumbing (Tchobanoglous et al., 2014). Petroleum-based oils such as kerosene, lubricant and asphalt contain basically carbon and hydrogen. When they enter a sewer system in an appreciable volume, the majority of these oils will float on the wastewater and have a greater propensity to coat water surfaces than fats, oils and soaps. These particles will invariably hinder biological actions. Also, they give rise to and cause maintenance problems by sticking onto walls and pipes, and consequently blocking filters and strainers (Diya'uddeen, Daud and Abdul Aziz, 2011).

As of now, various technical and management developments of oily wastewater are still unable to keep pace with the growth of Malaysia's industrial sector. Thus, the treatment techniques of oily wastewater have gained more attention in an effort to mitigate the impacts of oily wastewater on the environment. Several treatment methods have been developed extensively on the basis of achieving removal of a large amount of oil while considering the removal of other constituents. The oily wastewater treatment that has been put into conventional practice can be categorised into six approaches which are flotation, coagulation, biological treatment, electrocatalytic oxidation, supercritical water oxidation and membrane separation technology (Yu, Han and He, 2017).

Membrane separation technology, particularly polymeric membranes, has gained extensive attention in oily wastewater treatment among the techniques mentioned. Recent breakthrough in nanocomposite membranes is promising for oily wastewater treatment because membranes are enhanced in terms of hydrophilicity, antifouling performances, rejection efficiency, mechanical properties and thermal

stability (Ursino et al., 2018). Hence, they can be utilised in an eclectic range of process conditions. Nanocomposite membranes are generally prepared by incorporating nanofillers such as carbon nanotubes, graphene oxide, metal nanoparticles, etc into the polymeric matrix. These nanofillers may be either dispersed in the polymer solution or coated onto membrane surface before membrane casting (Ursino et al., 2018).

In this study, a polymeric membrane is fabricated by incorporating graphene oxide (GO) in nitrile butadiene rubber (NBR) via latex compounding and curing method. Even though the performances of NBR/GO membranes have been widely acknowledged in literature, the effect of degassing remains as a novel factor which attracts interest in moving one step ahead for practical application of the membrane in oily wastewater treatment. Therefore, this study compares the performances of both degassed and gassed NBR/GO membranes with respect to surface morphology, tensile properties, permeation flux and oil rejection efficiency.

## 1.2 Problem Statement

The conventional methods of oily wastewater treatment are demonstrating ineffective performances. For instance, flotation technique can barely separate oil droplets of size around 50 μm from wastewater. For even smaller droplet size, additional units are required to pretreat the wastewater before flotation (Santander, Rodrigues and Rubio, 2011). This will unavoidably entail a larger footprint and higher capital investments. Besides, formation of activated sludge is a problem from coagulation and biological processes because it is harmful when discharged into the open watercourse (Brandt et al., 2017). Poisons in certain wastewaters may also kill the microorganisms cultured for biological treatment. In advanced oxidation processes, the rate of reaction is affected by electrode passivation. Corrosion of electrode material is another limitation of using electrochemical catalysis for wastewater treatment (Anthuvan Babu et al., 2011). Supercritical water oxidation is hindered from being commercialised because salt precipitation on walls can plug the pipes and reactor. Heavy corrosion can also propagate from a dead zone between the salt layer and the wall (Ameta and Ameta, 2018).

Therefore, membrane separation technology is emphasised so as to take a step forward regarding the applications in oily wastewater treatment of late. Table 1.1 compares the feasibility of membrane technology for oily wastewater treatment with that of conventional treatment. Even though membrane treatment can attain high removal efficiency, other criteria as listed must also be considered when it comes to customising the best solution for some special needs.

**Table 1.1. Membrane Treatment vs Conventional Treatment (SUEZ Water Technologies, 2018).**

| | Membrane Treatment | Conventional Treatment |
|---|---|---|
| Footprint | Extremely compact | Large land requirement |
| Separation process | Physical barrier (reliable) | Gravity driven |
| Chemical use | Minimal | Intensive |
| Manpower | Fully automated | Intensive |
| Utility costs | High | Low |
| Operating costs | Not directly dependent on TDS | Highly dependent on TDS |
| Wastes | Solid waste and reject stream (20–30% of input stream) | Solid waste |

Even though membrane separation technology is superior to the conventional methods of treating oily wastewater, there are also some drawbacks of employing membranes. According to Asatekin and Mayes (2009), membrane fouling is invariable when subjected to heavy oily wastewater. The fact that oil components can easily block membrane pores imposes an arduous challenge to membrane applications in oily wastewater treatment. Besides, high rejection rate and high permeation flux can never be achieved simultaneously when using a membrane. One of the parameters have to be compromised. Thus, the optimal solutions to both permeation flux and rejection rate must be determined. Moreover, polymeric membranes have low mechanical strength, thermal stability and chemical resistance (Zavastin et al., 2010). This limits the applications of membranes in severe conditions.

For a technology to serve as an excellent oil removal practice, good chemical resistance, high rejection rate and high water flux must be fulfilled. However, the

existing polymeric membranes lack of these aspects as discussed. Hence, this research is carried out to study if graphene oxide (GO) is able to improve membrane performances. The polymer selected is nitrile butadiene rubber (NBR) as it can offer ideal chemical resistance and possesses superior mechanical strength due to its crosslinks. Meanwhile, GO selectively allows water to pass through the membrane provided that GO is hydrophilic in nature. As a result, the trade-off between rejection rate and water flux is expected to overcome after GO is incorporated. In the previous study conducted by Koay (2018), it was reported that 2 phr NBR/GO membrane was able to give the was able to give 92.23% of oil rejection rate while ensuring high water flux of 834.1 $L^2/(m^2 \cdot hr)$. In the previous study, the sulphur content was fixed at 1 phr.

The uses of latex compounding and curing method are actually novel although the development of polymeric membranes seems complete and omnifaceted. Thus, there are many parameters to be studied in order to optimise its performances. Incessantly, the area of development and studies are focused on thermal stability, mechanical strength, chemical and fouling resistance, water permeability, etc of a membrane. Since they can be enhanced by entailing graphene oxide, this research is made worthwhile. In this research, the degassing effect of latex before casting on the performance of the membrane is investigated into details. It is expected that the degassing process will affect the water flux and the rejection rate of oily wastewater treatment by altering the pore size of the membrane.

## 1.3 Objectives

i. To prepare nitrile butadiene rubber and graphene oxide composite membranes via latex compounding and curing method.
ii. To characterise the surface morphologies of both degassed and gassed NBR/GO membranes.
iii. To evaluate the tensile properties of both membranes.
iv. To study the degassing effect on oil rejection rate and water flux of both membranes.

# CHAPTER 2

# LITERATURE REVIEW

## 2.1 Petroleum Refinery Effluent (PRE)

Oily wastewater treatment has been a pain in every oilfield or petroleum company over past few decades. Especially for oil industry, petroleum refinery effluent (PRE) shares a considerable portion of waste generated by municipal and industrial sectors in Malaysia. The effluent quality in refinery wastewater depends on the operation procedures whereby hydro-cracker flare, hydro-cracking, hydro-skimmer flare, hydro-skimming, sourwater, condensate, condensate flare and the desalter are exemplified (Aljuboury, Palaniandy and Abdul Aziz, 2017). Table 2.1 as cited by Ishak and Malakahmad (2013) lists the typical characteristics of PRE. The organic matter in PRE, due in part to the presence of hydrocarbon groups, has become the principal concern in wastewater treatment because it shares more than 50% of constituents in PRE.

**Table 2.1. Typical Characteristics of PRE (Ishak and Malakahmad, 2013).**

| Parameter | Range (mg/L) | Mean (mg/L) |
|---|---|---|
| Chemical oxygen demand (COD) | 744–1673 | 1209 |
| Biochemical oxygen demand ($BOD_5$) | 205–448 | 327 |
| pH[a] | 7.50–9.41 | 8.46 |
| Turbidity[b] | 402–419 | 411 |
| Colour[c] | 3400–3650 | 3525 |
| Nitrate | 3.30–4.90 | 4.10 |
| Total suspended solids (TSS) | 280–340 | 310 |
| Alkalinity | 133–138 | 136 |
| Ammonia nitrogen | 40–45 | 43 |
| Oil and grease | 48–97 | 73 |
| Phosphorus | 1.67–1.73 | 1.70 |
| Total organic carbon (TOC) | 184–217 | 201 |
| Phenol | 1.16–1.44 | 1.30 |
| Sulphide | 14–17 | 16 |
| Sulphate | 40–50 | 45 |
| Total Kjeldahl Nitrogen (TKN) | 82–95 | 89 |
| Benzene | 33.31–34.36 | 33.85 |
| Toluene | 38.58–41.08 | 39.83 |
| Ethylbenzene | 1.80–1.90 | 1.85 |
| Xylene | 30.03–33.04 | 31.54 |

a = no unit, b = unit in NTU, c = unit in Pt Co

Low $BOD_5$ is shown because the materials can hardly be degraded by microbes, whereas high COD is resulted by the presence of easily oxidizable compounds by chemicals. In this case, the wastewater exhibits low biodegradability. Plus, the wastewater consists of oil and grease, as well as benzene, toluene, ethylbenzene and xylene (Ishak and Malakahmad, 2013). Other wastewaters originating from industries are invariably engaged in refining crude oil, lubricants and manufacturing fuels, which will also contribute to such conditions. If these non-biodegradable wastewaters are discharged to a watercourse without any pre-treatment, pollution of waterways will be

prompted because the constituents are fatal to aquatic life. Therefore, it is compulsory to purify the wastewater so that it can be reused to save water resources.

Enormous efforts have been invested in the search for the most effective way for oily wastewater treatment. As reported in literature, the most conventional methods for oily wastewater treatment such as flotation, coagulation, biological treatment and membrane separation technology are analysed so as to assess their removal performances of oil and grease.

## 2.2 Conventional Oily Wastewater Treatment

### 2.2.1 Flotation

Flotation is a unit operation that brings about the separation of solid or liquid droplets from a liquid phase by introducing air bubbles. More than facilitating the migration of particles with lower density to the liquid surface, the denser particles can also be made to float as a result of air buoyancy (Gupta and Yan, 2016). In oily wastewater treatment, oil droplets suspended in the water will adhere to the rising air bubbles. Once a froth layer of oil is formed on the water surface, it will be skimmed off and collected in a sludge hopper. The present practice of flotation is confined to the use of air as the flotation agent. Various chemical additives can actually be added in order to improve efficiency (Yargeau, 2012). An example of flotation unit is depicted in Fig. 2.1.

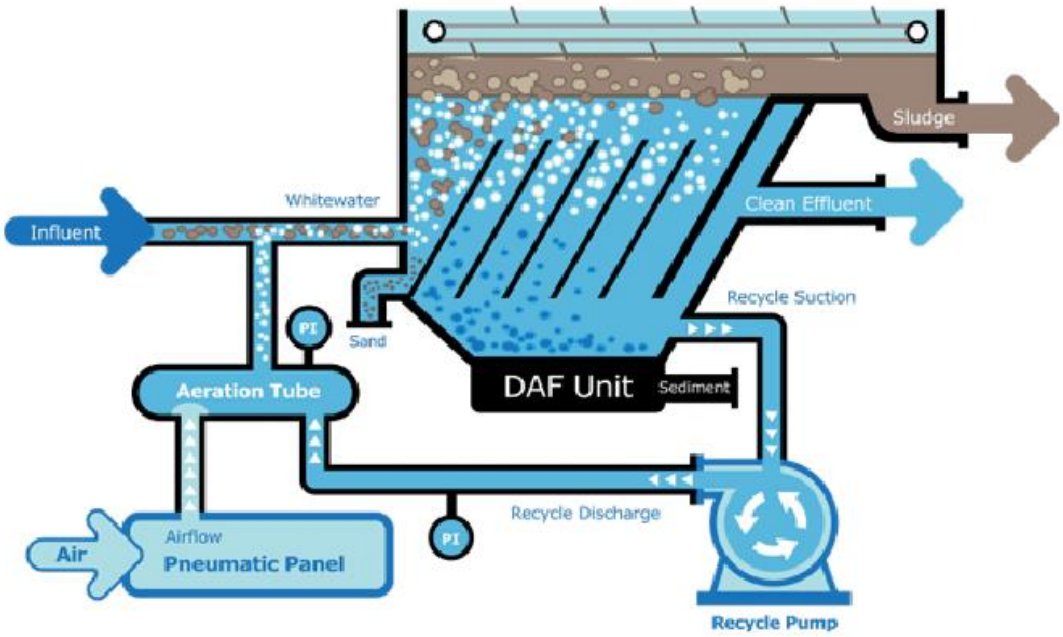


**Fig. 2.1. Schematic of Dissolved-Air Flotation System (JWC Environmental, 2019).**

Dissolved-air flotation and dispersed-air flotation are the most ubiquitous methods for the removal of stable oily emulsions, but both methods are being taken over by the jet flotation. According to Santander, Rodrigues and Rubio (2011), jet flotation requires no moving parts for scum removal. Thus, this technique is more beneficial than the conventional flotation methods because of easy installation and operation, low maintenance costs and low power consumption while offering generation of medium-sized bubbles (100–400 µm), high efficiency, high throughput, moderate equipment cost and safety features.

Flotation exhibits great potential in oily wastewater treatment owing to the low sludge generation, high throughput of modern equipment and the high efficiency of the separation schemes already available (Santander, Rodrigues and Rubio, 2011). However, the main drawback of using flotation is the intractable scum. Due to collection and adhesion factors, the fine droplets can hardly collide. Hence, it will encounter problems in phase separation when utilised for oil droplets of size around 50 µm. For the droplet size between 2–30 µm, fine bubbles and quiescent hydrodynamic conditions in the cell separation zone or emulsion breakers are usually

needed to pre-treat the wastewater before flotation (Santander, Rodrigues and Rubio, 2011).

As reported by Etchepare et al. (2017), dissolved-air flotation (DAF) was conducted to experiment on the separation of oil and water. Dismulgan, a cationic polyacrylamide, was added as the destabilising coagulant. Different effects of Dismulgan concentration, saturation pressure and bubble size on DAF performance were studied. The performance of DAF for oil–water separation was highest (99%) when the wastewater was flocculated with 5 mg/L of Dismulgan at pH 7 and saturation pressure of 5 bar with microbubbles and nanobubbles. The remaining oil concentration was less than 1 mg/L.

Painmanakul et al. (2010) combined induced air flotation (IAF) and coagulation to treat an oily wastewater that comprised anionic surfactant at critical micelle concentration. The removal efficiency increased with the alum concentrations until the optimum dosage of alum was reached. The highest removal efficiency of 99% in COD values was attained by the alum dosage between 800 and 1400 mg/L. In this experiment, the concentrations of alum required was high due to the entrapment in precipitates and the lower charge density of alum as compared with other coagulants. However, the process was inferior because of the extended operation times needed in mixing and sedimentation operations.

### 2.2.2 Coagulation

Oily wastewater usually comprises very large volumes of oil-in-water emulsions which are difficult to be separated from water because they are shielded from spontaneous coalescence into larger flocs. Typical colloidal particles found in wastewaters are negatively charged on the surface. The electrical charge exerts repelling forces that are larger than the attractive body forces between colloidal particles of size. The particle size is between 0.01 μm and 1 μm. Water molecules that are smaller in size cause constant thermal bombardment of the colloidal particles and

keep them in suspension (Tchobanoglous et al, 2014). As a result, simple gravity sedimentation for oily wastewater treatment can be extremely time-consuming.

Coagulation is hereby introduced to accomplish removals of emulsified oil and dissolved oil. A coagulant is a chemical added to destabilise the colloidal particles in wastewater for flocculation to occur upon particle collisions. Coagulants that are most conventionally applied in wastewater treatment are aluminium chloride, aluminium sulphate, ferrous sulphate, ferric chloride and hydrated lime. These chemicals are ubiquitous in treating colloids because of their high effectiveness, low costs, high handleability and easy availability (Aloui, Kchaou and Sayadi, 2009). Among the coagulants, aluminium species is most widely used for dewatering coagulation and sludge conditioning processes. Charge neutralisation occurs when the positively charged aluminium species that adsorb to negatively charged particles (Zhao, 2003). They are overdosed so as to maintain sufficiently high coagulation efficiency.

However, the formation of activated sludge gives rise to some environmental issues. Residual aluminium may be trapped by the activated sludge which is harmful when discharged into an open watercourse. Excessive consumption of aluminium salt may result Alzheimer's disease (Brandt et al., 2017).

The performance of a coagulant in oily wastewater cannot be predicted by theory due to the complex constituents in oily wastewater. Studies of a particular coagulant must be conducted by experiments. According to Zeng et al. (2007), poly-zinc silicate (PZSS) was synthesised by poly-silicic acid and zinc sulphate. It emerged as a new coagulant with cationic polyarcylamide and was applied in heavy oil wastewater treatment. The result showed that 100 mg/L of PZSS was able to achieve 95% of oil removal and almost 99% of suspended solids removal at pH 6.8. Poly-silicate radicle in PZSS assisted in coagulation and adsorption of the oil droplets by neutralising the negative charges of oil droplets to bind and bridge. As a result, a lower dosage of PZSS was required to destabilise the oil emulsions.

Ahmad, Sumathi and Hameed (2006) studied about the effects of mixing time on oil removal efficiency via coagulation of residue oil and suspended solids from palm oil mill effluent (POME) using chitosan. Dosages of chitosan, alum and poly-

aluminium chloride (PAC) were fixed at their optimum values which were 0.5 g/L, 8.0 g/L and 6.0 g/L respectively. Mixing time was manipulated over fixed mixing rate of 100 rpm. Then the content was allowed to settle for 1 hour. The result proved that a complete mixing of 15 minutes with chitosan was able to remove 99% of residue oil in palm oil mill effluent (POME), but alum and PAC took about 30 minutes to achieve this. When the mixing time was further increased to 1 hour for alum and PAC, the oil removal efficiency declined in turn. However, chitosan remained the same efficiency upon increasing the mixing time because it was able to adsorb the residue oil due to its amine functional groups.

### 2.2.3 Biological Treatment

Floating oil in water can be removed easily by filtration while oil-in-water emulsions can be treated by flotation or centrifugation. However, other dissolved components such as tiny oil droplets and dissolved hydrocarbons are difficult to treat. Biological treatment is capable of dealing with oil de-emulsification effectively and economically (Li, Kang and Zhang, 2005). It entails microbial metabolism to attain removal of dissolved and particulate carbonaceous BOD, and stabilisation of organic matter found in wastewater. Bacteria, yeast and fungi that are able to degrade crude oil can grow by consuming crude oil as carbon source. Biodegradation of crude oil by these natural microorganisms is one of the primary mechanisms by which hydrocarbons are eliminated from the environment (Li, Kang and Zhang, 2005).

There are various treatment processes for wastewater incorporating biological processes. First, activated-sludge process is a routinely used biological treatment of municipal and industrial wastewaters. This process exemplifies suspended growth treatment in which microorganisms stored in a tank are aerated non-stop so as to keep them in suspension form. The microorganisms decompose organic matter by adsorption to the surface of the activated sludge. An important feature of this process is the formation of settleable solids that can be removed by gravity settling (Wang et al., 2015). Secondly, biological filter method is a typical example of attached growth treatment. A non-submerged fixed biofilter is packed over which wastewater is

distributed continuously. As wastewater flows over the attached biofilm, organic pollutants will adsorb to the filter surface and be converted to harmless, stable substances by microbial decomposition (Tchobanoglous et al., 2014).

Li, Kang and Zhang (2005) studied the effects of using fungi and polyvinyl alcohol on the COD of oily wastewater. The highest rate of oil removal was reported when using *Bacillus* sp. M-12 as oil degraders and polyvinyl alcohol (PVA) were used to immobilise the bacteria cells. The COD was reduced from 2600 mg/L to 800 mg/L after 4 days.

A membrane bioreactor is another popular application of biological treatment in wastewater engineering because of its superior performances. It is modified from the conventional activated sludge process. The activated sludge is thickened in a bioreactor which is connected to a cross-flow ultrafiltration membrane unit. Ahmadi et al., (2019) examined the performances of a membrane bioreactor coupled with an ultrafiltration membrane unit to treat actual oil refinery wastewater with mixed liquor suspended solids (MLSS) concentrations of 6500 and 8500 mg/L and hydraulic retention times (HRT) between 12 and 24 hours. The highest COD removal of 97% was attained at the MLSS of 8500 mg/L and HRT of 24 hours.

Liu et al. (2013) adopted an upflow anaerobic sludge blanket (UASB) coupled with immobilised biological aerated filters (IBAFs) to treat heavy oil wastewater with large quantities of dissolved recalcitrant organic compounds and low nutrient of nitrogen and phosphorus. The COD, ammonia nitrogen ($NH_3$–N) and suspended solids in the wastewater were removed by 74%, 94% and 98%, respectively after running the system for 252 days. Most of alkanes were degraded by the UASB process, whereas the IBAF degraded organic compounds and removed the $NH_3$–N and suspended solids. These results suggested that the combined biotreatment system has large potential in large-scale treatment of heavy oil wastewater.

Zhao et al. (2006) entailed B350 M and B350 group microorganisms immobilised on carriers in a pair of biological aerated filter (BAF) reactors for the pre-treatment of oil field wastewater. The biodegradation system was operated for 142 days with a HRT of 4 hours and a volumetric load 1.07 kg COD $(m^3 \cdot d)^{-1}$. The reactor

which was immobilised with B350 M attained the average degradation efficiencies of 78% for TOC and 94% for oil. However, B350 could only attain 64% of TOC removal efficiency and 86% of oil removal efficiency.

Wu, Ge and Wan (2009) investigated the oil and COD removal efficiency of Yarrowia lipolytica W29 immobilised by calcium alginate. In this study, it was found that immobilised cells were superior to free cells in terms of thermostability. Besides, substrate concentration imposed significant effects on the degradability of immobilised cells. Yarrowia lipolytica W29 was able to achive more than 80% of oil degradation rate when the initial oil concentration was below 3000 mg/L. However, the oil degradation rate decreased upon further increasing the initial oil concetration. Storage stability and reusability tests discovered that the oil degradability of immobilised cells was stable when stored at 4°C for 30 days and reused for 12 times. The immobilised cells could maintain COD degradation rate of 82% at the sixth cycle. It was deduced that immobilised Yarrowia lipolytica had potential in wastewater treatment applications for the removal of oil and COD.

## 2.3 Membrane Filtration for Oily Wastewater Treatment

Membrane separation technology is a promising method to treat oily wastewater. Membrane is made of a special porous material that serves as a selective barrier to certain constituents. Based on the difference in pore size, membrane processes are generally divided into microfiltration (MF), ultrafiltration (UF), nanofiltration (NF) and reverse osmosis (RO). The specific pore size of a membrane allows undersized particles to pass through, and retains oversized particles (Couto, Lange and Amaral, 2018). Membrane separation follows the straining mechanism as illustrated in Fig. 2.2. In NF and RO, small particles are removed from water layer adsorbed on the surface of the membrane which is known as a dense membrane, whereas ionic species diffuse through the pores of the macromolecules composing the membrane (Tchnobanoglous et al., 2014).

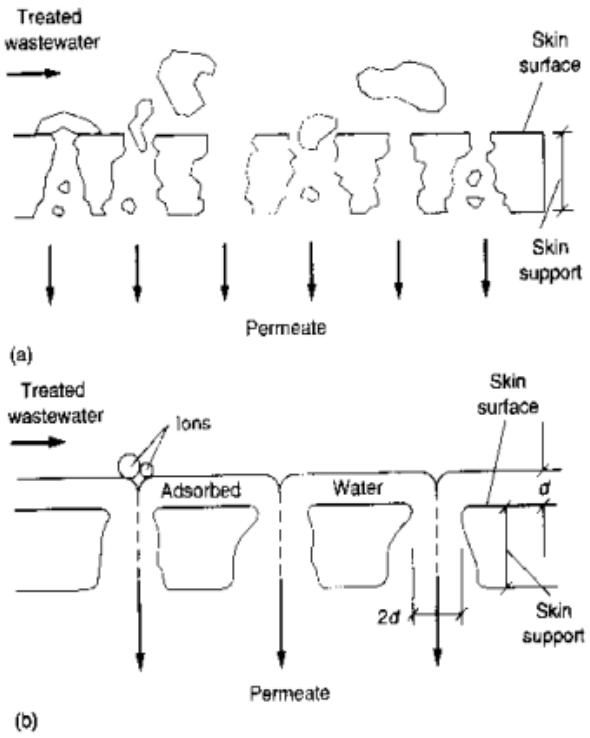


**Fig. 2.2. Definition Sketch for (a) Removal of Large Molecules and Particles by Straining and (b) Rejection of Ions by Adsorbed Water Layer (Tchobanoglous et al., 2014).**

The classification of membrane processes on the basis of size of separation is depicted in Fig. 2.3. There are considerable overlapping regions in the sizes of particles removed. MF is able to remove suspended particles, bacterial cells and some viruses; UF can retain colloidal materials and most of the disease-causing viruses; NF selectively blocks dissolved substances and multivalent ions; RO of finest pore size can virtually retain all constituents and allow only water to pass through.

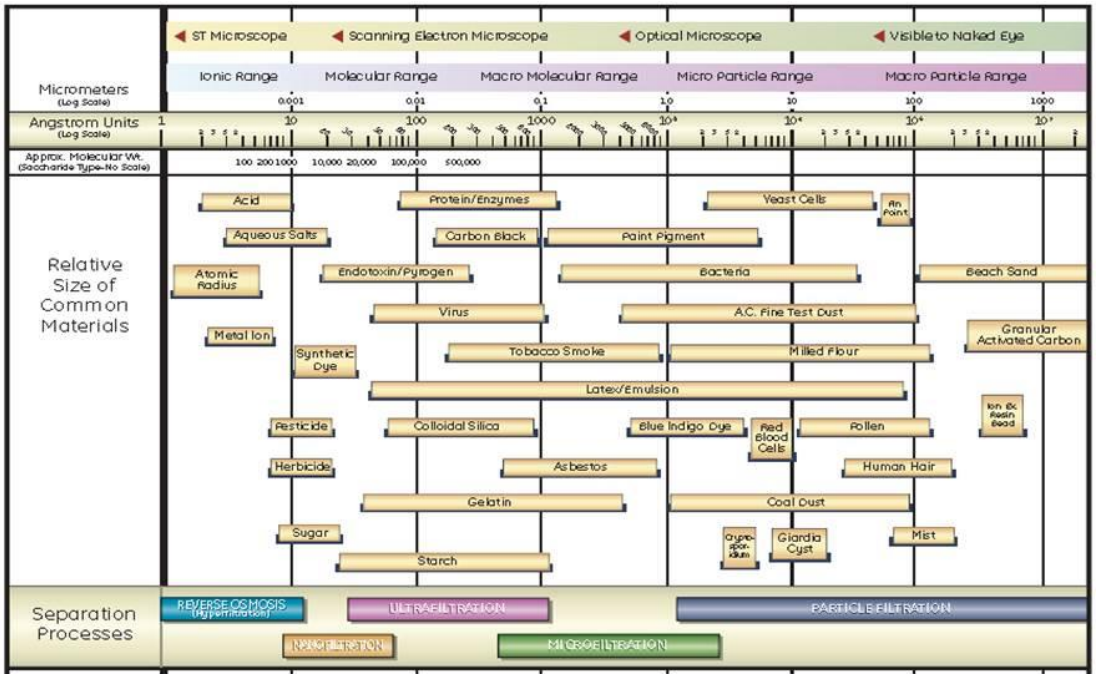


**Fig. 2.3. Comparison of the Size of the Constituents Found in Wastewater and the Operating Size Ranges for Membrane Technologies (MDA Filtration Inc, 2013).**

According to Tchobanoglous et al. (2014), membranes adopted for wastewater treatment are typically 0.20 to 0.25 μm thick and supported by a more porous structure of about 100 μm in thickness. Most commercial membranes are produced as fine hollow fibres, flat sheets, or in tubular form. There are two types of flat sheet membranes: asymmetric and composite. An asymmetric membrane is casted in one process. It consists of a thin layer supported on a thicker porous layer which allows high-flux filtration. A thin-film composite membrane is made by bonding a thin cellulose, polyamide, acetate, or other active layer to a thicker porous substrate in order to enhance stability.

Membranes are prepared from materials that can be classified into two major types: inorganic and organic. Inorganic membranes are made of ceramics, metals, or glass. They are superior to organic membranes owing to higher thermal, mechanical and chemical stability. Therefore, ceramic membranes are more suitable for operations under extreme conditions. The membranes used for wastewater treatment are typically made of organic materials such as aromatic polyamides, cellulose acetate,

polypropylene and thin-film composite. These polymeric membranes can offer better design flexibility and lower cost.

In Malaysia, a large quantity of oily wastewater is generated from industries. Oil-in-water emulsions are the most trying pollutants for which current treatment technologies are often ineffective and expensive. Recently, the applications of membrane processes have been mainstreamed in oily wastewater treatment owing to the advantages over the conventional methods.

Yu et al. (2006) looked into the membrane water permeations of a tubular UF module equipped with polyvinylidene fluoride (PVDF) membranes modified by inorganic nano-sized alumina particles to treat oily wastewater. After UF treatment, oil concentration was decreased from 15.5 mg/L to 0.25 mg/L, and suspended solids level was reduced from 15.8 mg/L to 0.2 mg/L with solid particle median diameter was less than 2 μm. The quality of the permeation water fulfilled the requirements by oilfield injection or drainage. The results indicated that the modified membrane permeation performance has been enhanced notably without compromising its retention properties.

Song et al. (2006) synthesised a coal-based MF carbon membrane by carbonisation of tubular carbonaceous precursor obtained via extrusion method. The highest oil removal efficiency was 97% when subjected to the optimum conditions: operating pressure of 0.10 MPa, pore size of 1.0 μm and flow rate of 0.1 m/s. The oil content after treatment was less than 10 mg/L which fulfilled the standards of national wastewater discharge.

Polysulfone (PSF) is a kind of popular membrane material for oily wastewater treatment because of its easy fabrication. Zhang et al. (2009) applied PSF to purify oily wastewater and examined its removal performances of oil. The membrane had been enhanced with sulfated Y-doped nonstoichiometric zirconia for better hydrophilicity and anti-fouling properties. The results revealed 99.16% of oil retention and 0.67 mg/L of oil content in the permeation, which met the discharge requirement. It was concluded that the composite membranes developed in the study possessed reasonable

fouling resistance, and thus the developed PSF membranes were feasible in treating oily wastewater.

A dynamic membrane from Kaolin and manganese dioxide ($MnO_2$) was developed by Yang, Ma and Yang (2011) to study the effect of different membrane-coating technique and different solution conditions on the performance of membrane. A Kaolin/$MnO_2$ bi-layer composite dynamic membrane is resulted because the $MnO_2$ particles deposited onto the surface of Kaolin dynamic layer. The dynamic membrane showed a high permeation flux and oil rejection efficiecy above 99% under neutral or alkaline conditions. The steady permeation flux was promoted from 120.1 to 153.2 $L/m^2 \cdot hr$ while the steady retention ratio reduced from 99.9% to 98.2% when the temperature increased from 283 K to 313 K.

In the research of Abadi et al. (2011), a tubular ceramic MF ($\alpha$-$Al_2O_3$) system was utilised for oily wastewater treatment. This system was able to produce a permeate with the oil concentration of 4 mg/L from the feed of 26 mg/L oil content. National Discharge Standard that required the discharge limit of oil below 10 mg/L was satisfied. TOC removal efficiency was approximately 95%. The optimal operating conditions to achieve the results were transmembrane pressure (TMP) of 0.125 MPa, cross-flow velocity (CFV) of 2.25 m/s and temperature of 32.5°C. The membrane was backwashed in this system so as to clean the membrane pores from oil and particulates. The backwashing was able to prevent the decline of permeate flux over operation time.

Mittal, Jana and Mohanty (2011) fabricated a hydrophilic ceramic–polymeric composite membrane from Kaolin, clay and a few binding materials for the treatment of oily wastewater. A study of effects of solution conditions on reflux decline was conducted. It was revealed that the rate of flux decline was directly proportional to the pressure. This was because collision between the emulsion droplet increased under pressurised conditions, thus larger droplet formed and created an oil layer over the membrane surface. Higher pressures forced the oil droplets into the pores and consequently promoted fouling. Similarly, higher initial oil content also resulted in higher flux decline. The maximum rejection was 93% at 41st minute produced a wastewater with 200 mg/L of initial oil concentration at 138 kPa. The final cost of the

composite membrane was much lesser than that of the available commercial membranes because the materials were obtained at low costs.

Salahi et al. (2013) used a nano-porous membrane (poly-acrylonitrile) sheet with nominal pore size of 10 nm for oily wastewater treatment in a desalter plant. The results signified high efficiency of nano-porous membrane for the treatment of petroleum refinery wastewater. The total dissolved solids, total suspended solids, oil and grease content and biochemical and chemical oxygen demands were decreased to 44.4%, 100%, 99.9%, 76.9% and 80.3% respectively. The treated water by the proposed method met the water quality required for irrigation or to discharge to the environment.

Another study conducted by Sarfaraz et al. (2012) looked into the performances of nano-porous membrane added with powdered activated carbon (NPM–PAC) in oily wastewater treatment. The results manifested that employing nano-porous membrane alone was not ideal in removing COD, TSS and TOC. Only 62.5% of COD removal and 75.1% of TOC removal were attained when the membrane was used individually. The steady permeation flux (SPF) was around 78.7 L/($m^2$ h). PAC was dosed optimally at 300 ppm to increase the removal of TOC and COD to 90.4% and 78.1% respectively, and the permeation flux up to 133.8 L/$m^2$·hr. PAC also reduced steady fouling resistance (SFR) around 46.1%. Therefore, a NPM–PAC hybrid membrane system was coupled with coagulation using PAC to achieve 90.2% and 97.6% for COD and TOC removals. The combination was effective in treating oily wastewater while improving permeation flux and membrane fouling resistance in the desalter plant.

## 2.4 Graphene Oxide (GO)

Graphene oxide is the nanofiller that will be studied extensively in this report. It is a carbon nanomaterial fabricated via exfoliation of graphite oxide (GtO). Upon exfoliation, the layered structure of GtO is interrupted and the interplanar distance between layers is increased. As illustrated in Fig. 2.4, the single layer of GtO which is rich in oxygenated functionalities is known as graphene oxide. Hydroxyl and epoxide groups are present in the basal planes while carboxyl groups exist at edges of plane (Singh, Kumar and Singh, 2016).

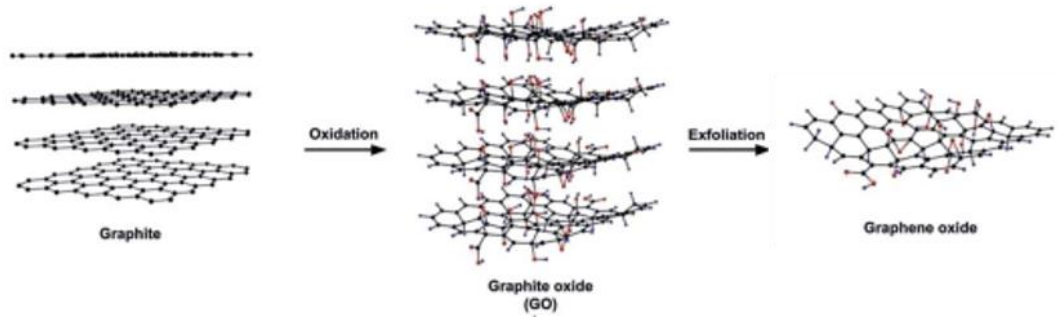


**Fig. 2.4. Preparation of Chemically Converted Graphene Oxide (Singh, Kumar and Singh, 2016).**

According to Ursino et al. (2018), graphene oxide has functional groups that can improve mechanical and thermal properties of a polymeric membrane by providing a variety of surface-modification reactions. There are various hydrophilic functional groups such as -OH, $-NH_2$ and $-SO_3H$ that can be useful to produce functionalised graphene- and graphene oxide-based materials. In recent years, graphene oxide has been applied in various water treatment processes including removal of toxic ions and organic molecules, water desalination and pharmaceutical traces from polluted water (Ursino et al., 2018).

These oxygenenated functionalities attribute to improved mechanical interlocking and better adhesion to the polymer chains. The GO sheets comprises both aromatic regions with unoxidised benzene rings and aliphatic regions with oxidised six-carbon rings where oxygenenated functionalities attach to. The bonds between

carbon and oxygen cause partial change of carbon atoms hybridisation from $sp^2$ to $sp^3$. As a result, the insulating properties of GO are imparted. Upon mixing, GO is able to disperse homogeneously in water while maintaining long-term stability in organic solvents since the oxygenated functionalities have high affinity to water molecules (Paredes et al., 2008).

The functional groups contribute to improvements in many aspects such as thermal properties, mechanical properties, hydrophilicity, antifouling properties, etc. Table 2.2 summarizes some research papers which study about GO incorporation in different types of polymer.

**Table 2.2. Incorporation of Graphene Oxide in Different Types of Polymer.**

| Polymer | Effect | Reference |
|---|---|---|
| Polysulfone (PSF) | • Improved thermal properties as a result of suppressed polymer chain mobility.<br>• At low GO content, the composite films underwent 3% of mass loss at 497°C, 500°C and 509°C as the GO content increased from 0% to 0.25% and 0.5% in weight.<br>• Improved E modulus by 16.58% and tensile strength by 18.02% as the GO content increased from 0.25 to 1 wt%.<br>• A strong interface required for an efficient load transfer from the matrix to GO was formed. | Ionita et al. (2014) |
| Polyamide | • Hydrophobic profile of the polymer was modified to hydrophilic due to the oxygenated functionalities from GO.<br>• The addition of 0.004 wt% GO to the neat polymer considerably increased the pure water flux from 18.66 $L/m^2 \cdot hr$ to 23.75 $L/m^2 \cdot hr$. | Xia et al. (2015) |

| | | |
|---|---|---|
| Polyvinylidene fluoride (PVDF) | • Enhanced reversible fouling resistance due to better detaching of the hydrophobic foulants from the hydrophilic membrane surface.<br>• After a ternary cycle of Bovine Serum Albumin (BSA) solution, inner fouling process and the flux recovery rate for PVDF/GO membrane was higher than the neat polymer membrane. | Xu et al. (2014) |
| Poly-ether sulfone (PES) | • Higher water permeability due to water affinity of GO.<br>• PES-GO membrane established 246 $L/m^2 \cdot hr \cdot bar$ of water permeability which outperformed most commercial UF membranes.<br>• More than 80% of rejection rates against serum albumin and methyl orange. | Jiang et al. (2015) |

## 2.5 Nitrile Butadiene Rubber (NBR)

NBR is classified as a thermoset rubber which distinguishes itself from a thermoplastic elastomer by the formation of cross-linking. The cross-linking irreversibly strengthens thermoset rubbers after being heated. Consequently, the products made of thermoset rubbers are resistant to melting and able to remain in shape upon heating. This nature of thermoset rubbers renders them the perfect properties that can avoid deformation in high-temperature applications. As illustrated in Fig. 2.5, NBR is a copolymer, comprising butadiene and acrylonitrile as their building blocks, which is produced by emulsion polymerisation via the action of free-radical initiators (El-hoshoudy, 2018).

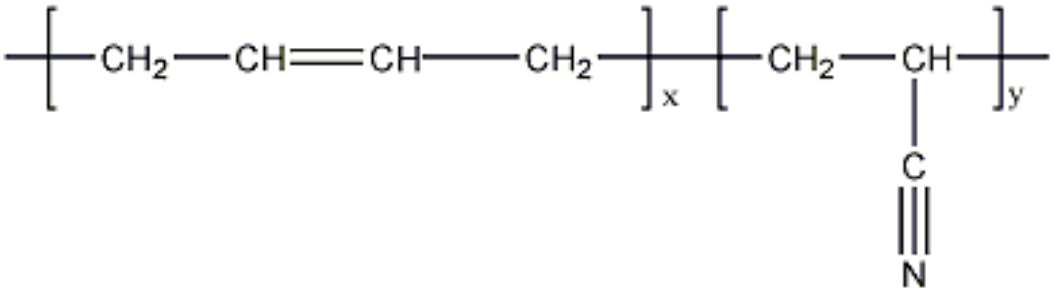


**Fig. 2.5. Butadiene and Acrylonitrile Units in a Chain of NBR.**

In wastewater applications, thermoset rubbers are more preferable than thermoplastic elastomers. The chains are held covalently by the curing agent as a result of the cross-linking between molecules. This makes most of the chemicals infusible and reinforces the structural integrity. Hence, thermoset rubbers can offer excellent resistance to chemicals and high temperatures. The other properties of thermoset rubbers are compared with those of thermoplastic elastomers in Table 2.3.

**Table 2.3. Comparison between Thermoset Rubbers and Thermoplastic Elastomers (Star Thermoplastics, 2018).**

| | Thermoset rubbers | Thermoplastic elastomers |
|---|---|---|
| Pros | • Resistant to higher temperatures<br>• Excellent aesthetic appeal<br>• Flexible design<br>• High level of dimensional stability<br>• Thick to thin wall design | • Recyclable<br>• Excellent impact resistance<br>• Capable of being remolded/shaped<br>• Superior aesthetic finishes<br>• Thick to thin wall parts<br>• Chemical resistant |
| Cons | • Not recyclable<br>• Cannot be remolded or shaped<br>• More scrap or waste from processing<br>• Difficult to surface finish | • Can melt if heated above melt point |

In the presence of heavy oil environment, NBR is favourably applied as it exhibits superior resistance to attack by oils. For instance, gaskets, automotive seals, or other items in contact with hot oils have ubiquitous applications of NBR. Therefore, NBR is selected as the material of polymeric membrane for the treatment of oily wastewater in this research. Acrylonitrile content is the key factor of controlling the polymer properties. The rubber can offer high strength, high resistance to swelling by hydrocarbon oils and low permeability to gases provided the content of acrylonitrile is high. Nevertheless, the rubber becomes stiffer at lower temperatures due to the higher glass transition temperature of polyacrylonitrile (Hanhi, Poikelispää and Tirilä, 2007).

The properties of a polymeric membrane can be improved with the employment of nanofillers. The effect of GO on the cure properties of NBR nanocomposites was analysed by Mensah et al. (2014). The scorch time increased in the initial vulcanisation of rubber after adding GO because the onset of vulcanisation was delayed by the nanofillers. The functional groups such as carboxylic acid and oxygen on the surface of the nanofillers absorbed the basic accelerator additives. Furthermore, another reason for the delay in the initial vulcanisation of the compounds was possibly a reason of the unrestricted chain mobility among the NBR system at the start of curing. When GO content was increased, the cure time became shorter because the filler was able to accelerate the vulcanisation reaction.

Mensah et al. (2014) prepared graphene oxide-reinforced acrylonitrile–butadiene rubber nanocomposites via solution mixing. Graphene oxide concentration was varied in the study. Upon the stress-strain tests, the sample with 2 phr of GO worked the best in terms of the elastic modulus and the tensile strength. The study manifested 8.1 MPa of tensile strength of the compound with 2 phr GO was recorded, which was 23% more than that of the neat rubber. It was deduced that a good GO dispersion through the matrix was able to enhance the interfacial interaction between rubber and GO.

Mensah et al. (2014) also described an outstanding thermal stability of NBR/GO nanocomposites because of the restrained chain mobility of polymer near the graphene surface. Inflammable anisotropic nanoparticles could form a jammed network of char layers that detained transport of the decomposition products when it

was subjected to combustion. The increased thermal stability again promoted the good GO dispersion and strong interfacial interaction between NBR matrix and GO.

It was also found that the cross-linking densities of NBR/GO nanocomposites could increase with the addition of GO because of strong interactions between the electron donating groups (hydroxyl) on the GO surfaces and the electron acceptor groups (acrylonitrile) in the NBR (Mensah et al., 2014). When the interactions between elastomer chains and the filler were strong, a single macromolecular chain could cover sizable quantities of active sites on the filler surface. Thus, there was a small number of chains attached to the surfaces. The unattached NBR chains might be contributing to the swelling of the elastomeric composite network. The effective filler-to-rubber links upon curing diminished the relative swelling ratio of NBR/GO compounds. The enhanced mechanical performance was influenced by the increased network (Mensah et al., 2014).

# CHAPTER 3

# METHODOLOGY

## 3.1 Materials

As illustrated in Fig. 3.1, the fabrication of NBR/GO membrane was started with the preparation of six raw ingredients: NBR latex, zinc oxide (ZnO), Sulphur (S), zinc diethyl dithiocarbamate (ZEDC), zinc mercaptobenzothiazole (ZMBT) and potassium hydroxide (KOH). NBR latex with a total solid content of 60% was supplied by Synthomer Sdn Bhd, Malaysia. The additives such as ZnO (47.7739%), S (55.4736%), ZEDC (56.7529%), ZMBT (58.3715%) in the form of aqueous paste, and KOH as solid pellets were obtained from Zarm Scientific & Supplies Sdn Bhd, Malaysia. NBR rubber was compounded with these additives which served their own functions as listed in Table 3.1.

**Table 3.1. Latex Compounding Ingredients and Their Functions.**

| Ingredient | Function |
|---|---|
| ZnO | ZnO is the most effective activator that increases vulcanisation rate with the accelerators such as ZEDC and ZMBT. By means of adsorption to ZnO surfaces, the interactions between compounding ingredients are improved (Coran, 2013). |
| S | S acts as the vulcanising agent for rubber which forms crosslinks between olefinically unsaturated bonds of adjacent molecular chains. Vulcanisation of rubber renders enhanced mechanical and ageing behaviour to the product (Joseph, 2013). |
| ZEDC | ZEDC is the primary accelerator that increases rate of vulcanisation and promotes low-temperature vulcanisation. It also allows the use of sub-quality sulphur without causing negative effects on rubber vulcanisation (Álvarez, 2018). |
| ZMBT | ZMBT is used as the secondary accelerator in combination with ZEDC. It contributes lower compression set, higher modulus and load bearing capacity to the enhanced properties of rubber products (Joseph, 2013). |
| KOH | KOH acts as the pH stabilizer or emulsifying agent. The latex must always be alkaline to prevent latex thickening or coagulation. Addition of KOH to NBR latex with stirring is able to produce a sufficient emulsion (Joseph, 2013). |

## 3.2 Process Flow Chart

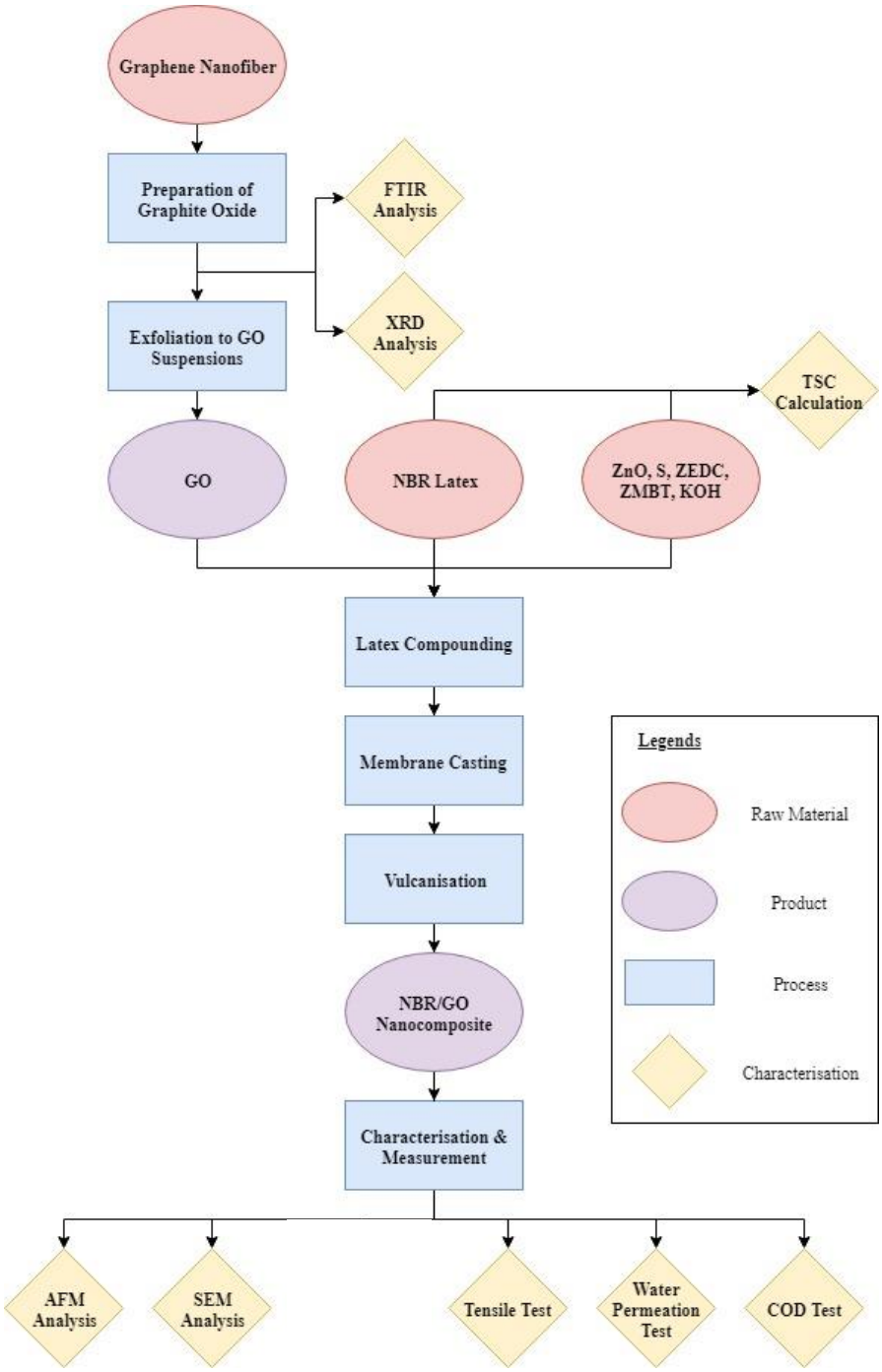


Where FTIR is Fourier-Transform Infrared Spectroscopy, XRD is X-Ray Diffraction, TSC is Total Solid Content, AFM is Atomic Force Microscopy, SEM is Scanning Electron Microscopy, COD is Chemical Oxygen Demand.

**Fig. 3.1. Process Flow Diagram of Synthesis, Characterisation and Testing of NBR/GO Membrane.**

## 3.3 Preparation of Graphene Oxide Suspensions

### 3.3.1 Preparation of Graphite Oxide

Synthesis of GtO was completed with modified Hummers method as cited by Bai et al. (2011). The procedure was started with harsh oxidation of graphene nanofiber (GNF) with concentrated sulphuric acid ($H_2SO_4$), sodium nitrate ($NaNO_3$) and potassium permanganate ($KMnO_4$). A measured 115 mL volume of concentrated $H_2SO_4$ (95–97%) was poured into a 500 mL beaker. The beaker was placed inside a basin of ice so as to maintain the temperature at 0°C. Simultaneously, the content was stirred at 400 rpm with a magnetic stirrer. As soon as the temperature was lowered to 0°C, 5 g of GNF and 2.5 g of $NaNO_3$ were added into $H_2SO_4$. Complete dissolution of $NaNO_3$ was ensured before continuining the oxidation. After that, 15 g of $KMnO_4$ was slowly added to the mixture. Because of the exothermic heat upon the addition of $KMnO_4$, the temperature was carefully controlled at 30°C. A dark green suspension as depicted in Fig. 3.2 was observed after the addition of $KMnO_4$. After another 10 minutes of stirring, the beaker was removed from the ice bath.

**Fig. 3.2. Dark Green Suspension Formed after the Oxidation of Graphene Nanofiber.**

The mixture was then allowed to stir at 500 rpm for 3 hours at room temperature. Then, 230 mL of deionised (DI) water was added gradually into the mixture. Due to the exothermic reaction, the DI water was added drop by drop so as to maintain the temperature at 70°C. Once the addition of DI water was complete, the mixture was stirred for additional 10 minutes. Then, the mixture was transferred to a 1 L beaker and further diluted with 700 mL of DI water. The mixture was dispersed into the DI water by a spatula. A measured 12 mL volume of hydrogen peroxide ($H_2O_2$) was added into the mixture, and a light-yellow suspension was observed indicating the formation of GtO. At the end of the oxidation step, the mixture was left overnight in the fume hood for sedimentation.

After sitting overnight, the mixture was filtered by a multichannel manifold filter. Each channel was equipped with an Anodisc membrane of 0.1-micron pore size. The mixture was poured onto the membrane and a vacuum suction was applied. At the same time, 5% of hydrochloric acid (HCl) was prepared from 37% of HCl through dilution with DI water. After completing the filtration, a moist layer of filter cake was formed on the membrane. The filter cake which was rich in GtO was collected in a 250 mL beaker, whereas the filtrate was discarded. The filter cake was then washed by immersing the filter cake in a beaker of diluted HCl. Once again, the mixture was filtered with the Anodisc membrane to obtain the filter cake. The process was repeated for a few times by washing with DI water instead of the diluted HCl. Upon completing the filtration step, the mixture was concentrated with GtO and the acidity was mitigated.

The concentrated mixture was poured evenly into six centrifuge tubes by ensuring all of the tubes sharing the same mass. The tubes were inserted symmetrically into the tube holes of a versatile refrigerated centrifuge (CT15RT) supplied by Techcomp Group. The rotor was placed properly on the drive shaft in such a way that the rotor was balanced in the chamber. Then, the door was closed. The centrifuge was allowed to run at 14000 rpm at room temperature for 30 minutes for each cycle. After 30 minutes, the content of each centrifuge tube was separated into two layers as shown in Fig. 3.3. The clear supernatant was carefully decanted from each tube, leaving the precipitate which was GtO at the bottom. The precipitate was scraped from each tube using a pair of forceps and collected in a 250 mL beaker. In order to remove its acidity,

the collected precipitate was washed with DI water and the pH was tested with a piece of pH indicator paper after each cycle of centrifuge. The centrifuge procedure was repeated for several times until the pH value of the sample was increased to 5–7. Once the desired pH was obtained, the GtO was removed from water by performing one last cycle of centrifuge. The collected sample was dried in a drying oven (UNB 500), supplied by Memmert at 60°C overnight to completely remove water from the precipitate. The dried precipitate must be characterised using FTIR and XRD so as to ensure the presence of particular functional groups.

**Fig. 3.3. Two Separated Layers after Performing a Centrifuge Cycle.**

### 3.3.2 Exfoliation of Graphite Oxide to Graphene Oxide Suspensions

Mechanical exfoliation is the most common approach to obtaining graphene oxide (GO) from GtO. Following the synthesis of GtO, it was subjected to ultrasonication so as to break the weak van der Waals forces that held the layers together. Ahead of the exfoliation, the dried GtO was first mixed with DI water at a weight ratio of 1:3 so as to give a mixture with 25% of total solid content. The GtO was kept in suspension form by stirring with a spatula. As depicted in Fig. 3.4, a probe-type ultrasonic homogeniser (Q500) supplied by QSonica was used to perform exfoliation of GtO. The probe tip was immersed into the sample mixture inside the ultrasonic homogeniser. The probe was immersed to a depth that was at least 1.5 times the tip diameter in order to prevent foaming in the sample. The process was allowed to run for 30 minutes to disentangle the sheets that tended to cling together and form lumps. A paste-like mixture, which was graphene oxide, was obtained after 30 minutes. The sample could be readily used for latex compounding.


**Fig. 3.4. Probe-Type Ultrasonic Homogeniser.**

## 3.4 Preparation of NBR/GO Membranes

### 3.4.1 Total Solid Content (TSC) Calculation

Total solid content (TSC) is the percentage of weights obtained before and after the drying process at a definite temperature. Each of the ingredients for latex compounding was supplied in the form of suspension. Thus, TSC calculation was performed on them ahead of latex compounding so as to determine the dry weights.

The procedure was started with the preparation of the ingredients. Five empty crucibles were labelled accordingly, and the weight of each empty crucible ($W_{crucible}$) was determined. NBR latex, ZnO, S, ZEDC and ZMBT were transferred into the crucibles in small quantities, separately. The crucibles were again weighed after filled with the ingredients ($W_{crucible} + W_{wet}$). As such, the weight of each wet sample ($W_{wet}$) could be calculated by using Eq. 3.1.

$$W_{wet} = (W_{crucible} + W_{wet}) - W_{crucible} \quad \text{(Eq. 3.1)}$$

The ingredient preparation was followed by drying in an oven at 105°C. After 2 hours, the crucibles were allowed to cool to room temperature and weighed on an electronic balance. After weighing, the crucibles were again placed inside the oven for drying. They were repetitively dried, cooled and weighed at two-hour intervals until a steady weight was obtained. A total removal of water was indicated by the constant weight ($W_{final}$). After the drying process, the TSC was finally determined by using Eq. 3.2.

$$TSC = \frac{W_{final} - W_{crucible}}{W_{wet}} \times 100\% \quad \text{(Eq. 3.2)}$$

KOH was bought as translucent pellets. In order to produce a KOH solution of 10% TSC, the KOH pellets were mixed and dissolved completely in DI water at a weight ratio of 1:9. All data involved in TSC calculation were recorded in Table 3.2.

**Table 3.2. Weight and TSC Measurements of Ingredients for Latex Compounding.**

| Ingredient | Weight (g) | | | | | TSC (%) |
|---|---|---|---|---|---|---|
| | $W_{crucible}$ | $W_{crucible} + W_{wet}$ | $W_{wet}$ | $W_{final}$ | Dry weight | |
| NBR | 67.4938 | 68.5064 | 1.0126 | 68.1239 | 0.6301 | 62.2260 |
| ZnO | 87.4799 | 88.6636 | 1.1837 | 88.0454 | 0.5655 | 47.7739 |
| S | 60.2294 | 60.9611 | 0.7317 | 60.6353 | 0.4059 | 55.4736 |
| ZEDC | 71.9249 | 72.6320 | 0.7071 | 72.3262 | 0.4013 | 56.7529 |
| ZMBT | 94.5801 | 95.7603 | 1.1802 | 95.2690 | 0.6889 | 58.3715 |

### 3.4.2 Latex Compounding

The preparation of the NBR/GO membrane was attained via latex compounding method. The formulation based on parts per hundred rubber (phr) as listed in Table 3.3 was suggested to compound the ingredients. According to Koay (2018), S of 1 phr and GO of 2 phr were incorporated into NBR latex to achieve the best performances in terms of the mechanical properties and the water flux.

**Table 3.3. NBR Latex Formulation.**

| Ingredient | Formulation (phr) | TSC (%) | Dry weight (g) | Moisture weight (g) |
|---|---|---|---|---|
| NBR | 100.0 | 62.2260 | 62.2260 | 100.0 |
| ZnO | 1.0 | 47.7739 | 0.6223 | 1.3026 |
| S | 1.0 | 55.4736 | 0.6223 | 1.1218 |
| ZEDC | 1.0 | 56.7529 | 0.6223 | 1.0965 |
| ZMBT | 0.5 | 58.3715 | 0.3111 | 0.5330 |
| KOH | 1.0 | 10.0 | 0.6223 | 6.2230 |
| GO | 2.0 | 25.0 | 1.2445 | 4.9780 |

From Table 3.3, each ingredient weight on a wet basis was determined and prepared accordingly. Then, the designed amounts of the ingredients were added into

a 250 mL beaker following the sequence: NBR latex, half of the KOH solution, ZnO, ZEDC, ZMBT, GO and S. The residues sticking to the wall of the glassware were recovered into the compound by washing with the remaining KOH solution. At the same time as the ingredients were added, the compound was homogenised by an overhead stirrer at a speed between 250–300 rpm. After stirring for 30 minutes, the compound was ready for membrane casting.

Two latex compounds of the same formulation were prepared. In order to study the degassing effect on the performances of latex-based membranes, a vacuum suction was applied to one of the compounds for degasification. The latex compound was placed inside a vacuum oven (TVAC-53), supplied by Tech-Lab Scientific, for 20 minutes to remove entrapped air. On the contrary, the other one was directly sent to membrane casting without being degassed by the vacuum oven. To avoid confusion, the membrane without being degassed is termed “gassed” membrane throughout the research paper. It is remarked that the “gassed” membrane did not undergo any procedure specifically for air induction into the latex.

### 3.4.3 Membrane Casting

Membrane casting was accomplished by using a lab-scale membrane auto casting machine (A4K-S564) from Autonics. The setup of the machine was demonstrated in Fig. 3.5. First, a glass plate was placed on top of the machine. The casting knife was adjusted to a gap of 0.05 mm and placed on the glass plate. The casting parameters were controlled at a distance of 220 mm and a forward speed of 150 rpm for both latex compounds. Next, the latex compound was poured into the casting knife onto the glass plate. The machine was started right after the latex compound was poured onto the glass plate. Within a few seconds, a thin film of the latex compound with an approximate thickness of 0.05 mm was coated on the glass plate. After the membrane was casted on the glass plate, it was vulcanised inside a convection oven at 70°C for 2 hours.


**Fig. 3.5. Membrane Auto-Casting Machine.**

## 3.5 Characterisation Methods

### 3.5.1 Fourier-Transform Infrared Spectroscopy (FTIR)

FTIR analysis was conducted on GNF and GtO by using Spectrum RX I supplied by PerkinElmer so as to detect the functional groups existing inside the molecular structures. The analysis was performed to identify the absorption bands produced by the chemical bonds inside GNF and GtO within a specific range on the infrared spectrum. The pre-set parameters were 4 scans with 4 $cm^{-1}$ resolution and a measurement range of 400–4000 $cm^{-1}$. Both samples must be prepared ahead of the analysis. Each of them was pulverised with potassium bromide (KBr) powder at a volume ratio of 1:10. Then, it was pressurised inside a pellet-forming die to produce a thin sheet that was transparent in the infrared region. Background spectrum was captured before the samples were scanned.

### 3.5.2 X-Ray Difraction (XRD)

X-Ray Diffractometer (XRD 6000) from Shimadzu was adopted to perform XRD analysis on GNF and GtO. Via Nickel filtered Copper Kα radiation with a wavelength of 0.154 nm, the interlayer spacing and crystallinity of GNF and GtO were measured. The samples were scanned under a rate of 2°/min between 10–60°. Bragg's Equation as shown in Eq. 3.3 was applied to calculate the interlayer spacing.

$$d = \frac{n\lambda}{2\sin\theta} \qquad \text{(Eq. 3.3)}$$

where

$d$ = Interlayer spacing, Å

$\lambda$ = Wavelength, nm

$\theta$ = Maximum diffraction angle, °

### 3.5.3 Field Emission Scanning Electron Microscopy (FESEM)

FESEM was adopted to examine the surface morphologies at the nanoscale of both gassed and degassed NBR/GO membranes in terms of GO dispersion, wrinkles, ripples, pore size, etc. The equipment model available for the study was JSM 6701F supplied by JEOL Ltd. Sputter coating was the only sample preparation required prior to the analysis. The samples must be coated with platinum particles to avoid accumulation of electrons on the surface. Then, the surface morphologies of the samples were observed under a microscope at different powers of magnification: 200×, 500×, 1000×, 5000×, etc.

### 3.5.4 Atomic Force Microscopy (AFM)

A non-contact mode AFM (XE-70) supplied by Park Systems as shown in Fig. 3.6 was used to analyse the surface roughness of the NBR/GO membranes. The sample was held in place on the sample holder by a double-sided tape. Then, the sample holder was mounted on the stage beneath the cantilever. The sample surface was approached by using the Z-stage control window to a few mm away from the tip. The optical microscope was adjusted to focus on the sample. The x/y stage controls were adjusted to move the sample to desired area. The scan size was set to 10.0 µm × 10.0 µm.


**Fig. 3.6. Atomic Force Microscope.**

After the sample was ready, the scan parameters were optimised to improve tracking. Scan rate, Z servo gain, set point and drive were adjusted to a point that a good image was achieved when the same topography was displayed by trace and retrace. After that, the scanning was initiated. The tip was oscillated at a given frequency above the sample surface. A few minutes were taken to complete the scan. At the end of the scan, 2D and 3D images of the sample, as well as the statistics on surface profile, were retrieved from the system. It was noted that the AFM was highly sophisticated and sensitive, so extra care must be taken when operating the instrument.

## 3.6 Performance Tests

### 3.6.1 Tensile Strength Test

Tensile strengths of both gassed and degassed membranes were inspected by using a light-weight tensile tester (H10KS-0748) supplied by Tinius Olsen as presented in Fig. 3.7. The test was performed on the samples at ambient conditions. The purpose was to study the degassing effect on the mechanical properties of a latex-based membrane in terms of elastic modulus, ultimate tensile strength and elongation at break.

**Fig. 3.7. Light-Weight Tensile Tester.**

Before conducting the test, the dumbbell-shaped specimens as depicted in Fig. 3.8 were prepared using a dumbbell press cutter. Each specimen was dimensioned into a gauge length of 26 mm and a neck width of 3 mm. The thickness was measured particularly with a digital micrometer. The dimensions of each specimen were recorded in Table 3.4. After clamping onto the tensile tester, the specimen was subjected to a load setting of 450 N, an extension length limit of 1200 mm and a stretching speed of 100 mm/min. The test was aborted as soon as the specimen was broken.

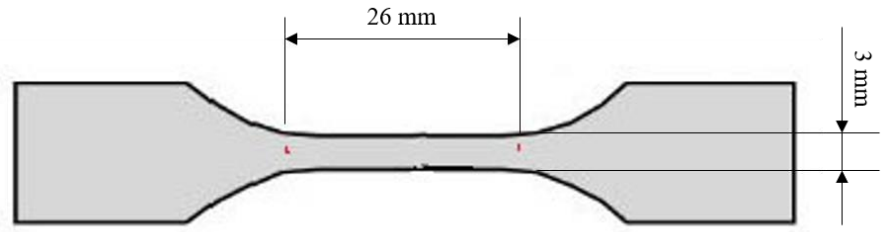


**Fig. 3.8. Dumbbell-Shaped Specimen.**

**Table 3.4. Dimensions of Gassed and Degassed Specimens for Tensile Strength Test.**

| Specimen | Gage length (mm) | Neck width (mm) | Thickness (mm) | Cross-sectional area ($mm^2$) |
|---|---|---|---|---|
| Degassed NBR/GO membrane | 26 | 3 | 0.082 | 0.246 |
| Gassed NBR/GO membrane | 26 | 3 | 0.078 | 0.234 |

### 3.6.2 Permeation Flux Test for Synthetic Oily Wastewater

The test was started with the preparation of synthetic oily wastewater. The required materials were diesel oil purchased from Petron Corporation, sodium dodecyl sulphate (SDS) as the surfactant and DI water. A synthetic oily wastewater with the oil content of 1000 ppm was prepared by homogenising 1 g of diesel oil with 1 L of DI water, feeding along with 0.01 wt% of SDS. The reason of imparting the oil content of 1000 ppm was because typical oily wastewater had already been treated to the levels between 50–1000 ppm of total oil and grease (TOG) concentration in processes upstream of membrane filtration. In order to investigate the membrane performance when subjected to different concentrations of oil, a synthetic oily wastewater with 500 ppm of oil content was also prepared.

The emulsification of diesel oil was attained by utilising the probe-type ultrasonic homogeniser (Q500) supplied by QSonica. About 30 minutes were taken to emulsify the synthetic oily wastewater until no visible phase separation. The appearance of the synthetic oily wastewater upon completion of preparation was illustrated in Fig. 3.9.

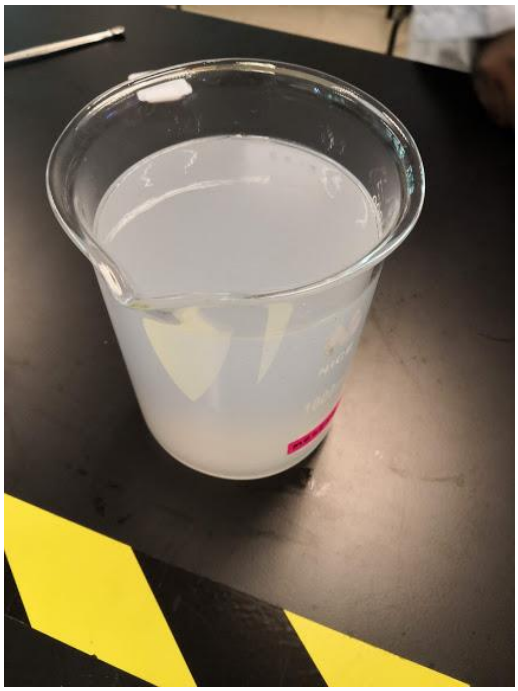

**Fig. 3.9. Appearance of Synthetic Oily Wastewater.**

The oil particle size in water was estimated by using a particle counter (LIGHTHOUSE, LS-20). Size readings in eight different size channels of 1.0, 2.0, 5.0, 7.0, 10.0, 15.0, 25.0 and 50.0 μm were provided upon measuring size of oil droplets. It was concluded that all droplets fell within the specified range between 1.0–50.0 μm with majority of droplet size revolving around 7 μm.

Then, permeation flux test was performed on the membranes with the synthetic oily wastewater which had been prepared in advance. An effective separation of oil from water was presumed to be achieved in a dead-end membrane test rig as shown in Fig. 3.10. In this study, the gassed and degassed membranes were subjected to different pressures and oil concentrations in order to investigate the degassing effects on oil

rejection efficiency and water flux under various conditions. The synthetic oily wastewater was pressurised through the membranes by nitrogen gas.


**Fig. 3.10. Dead-End Membrane Test Rig.**

The main aim was to determine the permeate flux that could be achieved by the gassed and degassed membranes at different pressures. Permeate flux was calculated by using Eq. 3.4. The membrane used for the filtration cell was fixed to a mandatory nominal diameter of 50 mm. Thereby, the effective membrane area for permeate flux calculation was controlled at $1.0179 \times 10^{-3}$ $m^2$. Besides, the time taken to collect 30 mL of filtrate was recorded for the calculation. The filtrate was preserved for subsequent COD test which was able to manifest the oil rejection efficiency.

$$J_p = \frac{V_p}{A \times t} \qquad \text{(Eq. 3.4)}$$

where

$J_p$ = Permeation flux, $\frac{L}{m^2 \cdot hr}$

$V_p$ = Permeate volume collected, $L$

$A$ = Effective membrane area, $m^2$

t = Time taken to collect the measured volume of permeate, $hr$

### 3.6.3 Chemical Oxygen Demand (COD) Test

COD is one of the crucial parameters to determine the removal efficiency of certain wastewater constituent. In this study, the COD test was conducted to find out the oil rejection efficiencies that were able to be achieved by the membranes. According to Eq. 3.5, oil rejection efficiency was obtained by comparing the COD values of the synthetic oily wastewater and the filtrate.

$$R = \left(1 - \frac{COD_p}{COD_f}\right) \times 100\% \qquad \text{(Eq. 3.5)}$$

where

$R$ = Oil rejection efficiency, %

$COD_p$ = COD level in permeate, $mg/L$

$COD_f$ = COD level in wastewater feed, $mg/L$

The COD test was carried out in two stages: reactor digestion and colorimetric procedures. The reactor digestion procedure was started with the preparation of a blank cell. DI water was measured to a volume of 2 mL and added into a High Range Plus COD digestion reagent vial supplied by Hach Company. It was noted that the unused vials must be stored inside a closed box because the reagents were sensitive to light. The vial was held by the cap and inverted gently for several times to mix. The collected filtrate and the synthetic oily wastewater were also prepared in the same way. All of the vials were labelled accordingly and put into the preheated COD reactor (Hach DRB 200). The samples were digested by the COD reagents at 150°C for 2 hours. Colour changes in the samples were noticed after two-hour reaction. The vials were allowed to cool to room temperature.

The colorimetric procedure was performed by DR-6000 UV-Vis Spectrometer. Program 435 COD HR was selected on the instrument. The sample cell must be cleaned with a tissue paper every time before inserted into the cell holder of the spectrometer. One blank must be run with each set of samples. The blank was inserted into the cell holder to zero the instrument. The COD values of the samples were then read by the instrument and the results were recorded.

# CHAPTER 4

# RESULTS AND DISCUSSION

## 4.1 Characterisation of Graphene Nanofiber and Graphite Oxide

### 4.1.1 FTIR Analysis

FTIR was performed to distinguish GtO from GNF. The FTIR spectra of GNF and GtO are presented in Fig. 4.1.

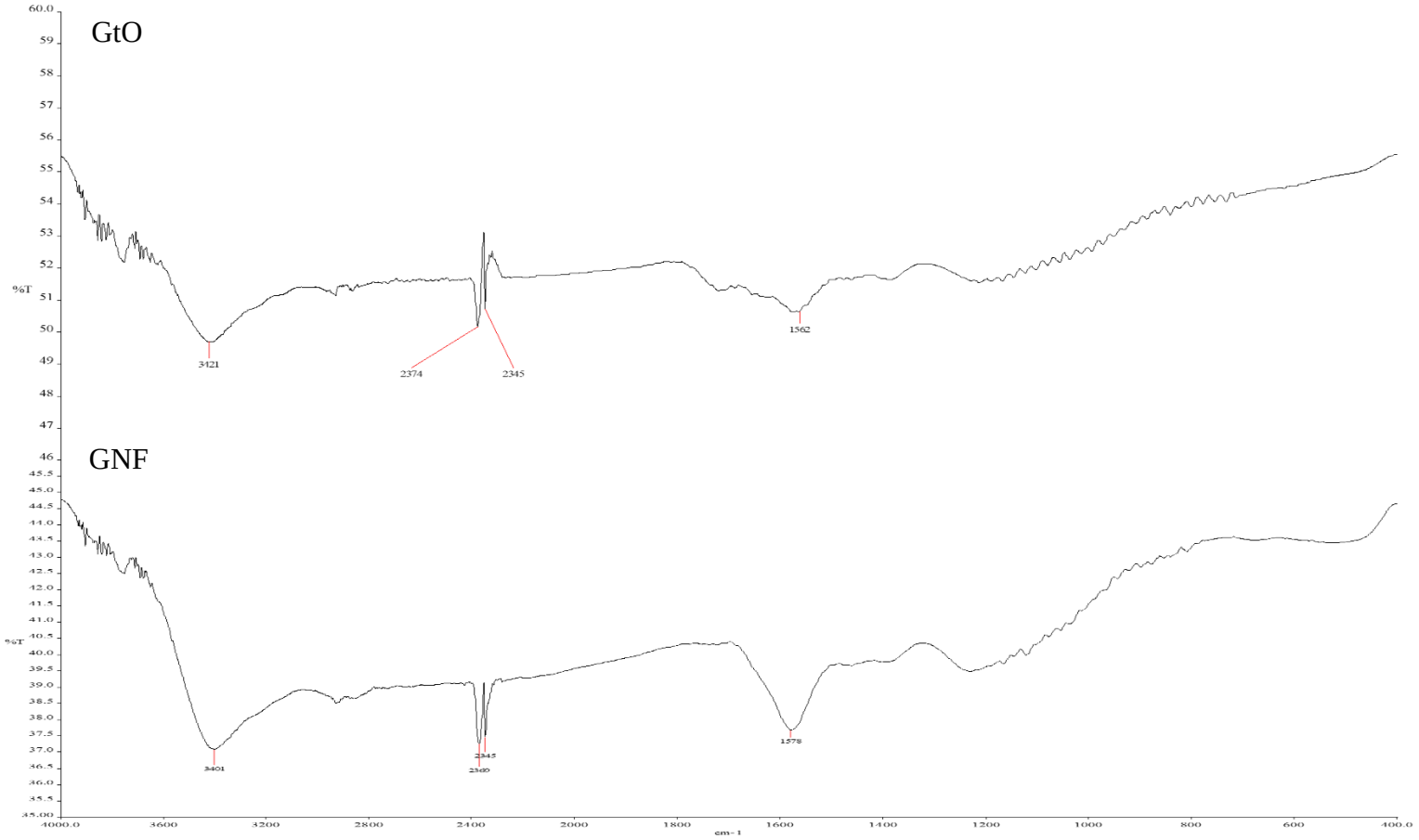


**Fig. 4.1. FTIR Spectra of Graphene Nanofiber and Graphite Oxide.**

As depicted in Fig. 4.1, the FTIR spectrum of GNF reveals the most remarkable appearance of strong absorption band at 1578 $cm^{-1}$. This peak justifies the presence of C=C stretch of aromatics (Qureshi and Panesar, 2019). Moreover, there is also a peak which falls within the range between 1290–1430 $cm^{-1}$. This peak indicates the presence of C-H in-plane bend of alkenes (Qureshi and Panesar, 2019). The doublet band at around 2300 $cm^{-1}$ describes the absorption of background $CO_2$.

As compared with GNF, GtO contains many oxygen-containing functional groups. According to Fig. 4.1, the presence of ethers can be confirmed by C-O-C stretch between two alkyl groups at the range of 1000–1300 $cm^{-1}$. Epoxide and carbonyl groups are also detected from the sample as a result of the peaks that represent C-O stretch (1210–1320 $cm^{-1}$) and C=O stretch (1700–1730 $cm^{-1}$), respectively. The presence of hydroxyl groups is demonstrated by O-H stretch that is found at the peak with absorption band of 3421 $cm^{-1}$ (Qureshi and Panesar, 2019). These oxygen-containing groups prove that the conversion of GNF to GtO has been a success. The interpretations of the FTIR spectra are summarised in Table 4.1.

**Table 4.1. Analysis on FTIR Spectra of Graphene Nanofiber and Graphite Oxide.**

| Functional group | Molecular motion | Wavenumber ($cm^{-1}$) | Graphene nanofiber | Graphite oxide |
|---|---|---|---|---|
| Alkenes | C-H in-plane bend | 1290–1430 | ✓ | ✓ |
| Aromatics | C=C stretch | ~1475 & ~1600 | ✓ | ✓ |
| Carbon dioxide | $CO_2$ | ~2300 | ✓ | ✓ |
| Ethers | C-O-C stretch (dialkyl) | 1000–1300 | × | ✓ |
| Epoxide | C-O stretch | 1210–1320 | × | ✓ |
| Carbonyl | C=O stretch | 1700–1730 | × | ✓ |
| Hydroxyl | O-H stretch | 3300–3400 or ~3650 | × | ✓ |

### 4.1.2 XRD Analysis

XRD analysis was performed to support the conversion from GNF to GtO. Fig. 4.2 illustrates the XRD diffractograms for both GNF and GtO. A sharp reflection of GNF is observed at 2θ = 26.3281°, corresponding to the interlayer spacing of 0.3382 nm. After harsh oxidation, the peak shifts to a lower angle at 2θ = 12°, corresponding to the interlayer spacing of 0.7366 nm. The larger interlayer spacing implies the intercalation of oxygenated functionalities embedded in the layers, whereas the reduced intensity indicates the exfoliated nature of GtO (Malas, 2017).

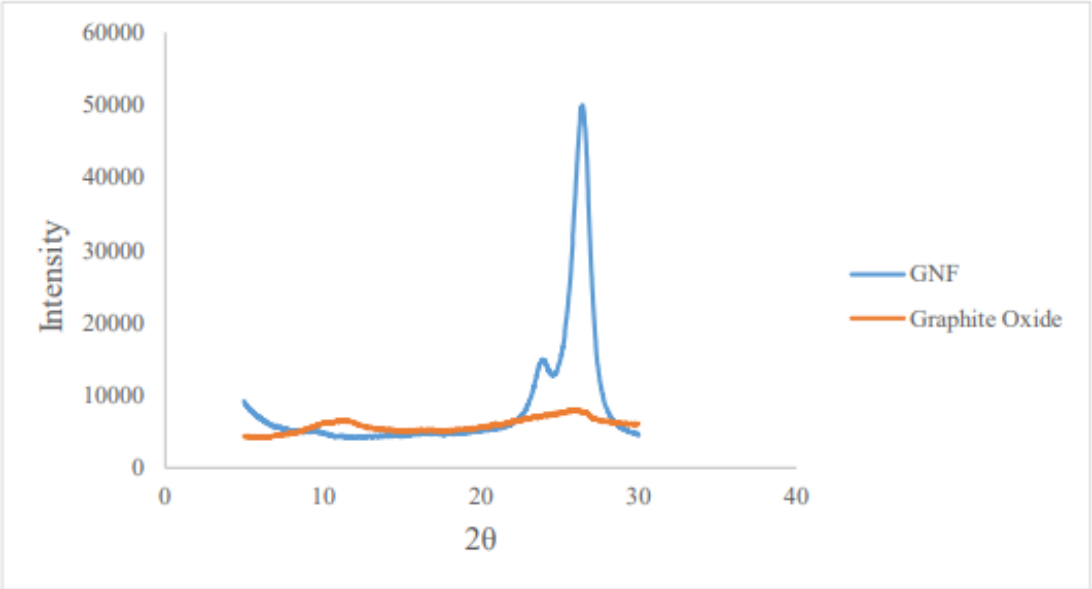


**Fig. 4.2. XRD Diffractograms of Graphene Nanofiber and Graphite Oxide.**

## 4.2 Morphologies of Degassed and Gassed NBR/GO Membranes

### 4.2.1 FESEM Analysis

Both degassed and gassed membranes were observed using FESEM in order to study their surface morphologies. For instance, folds and pores are the key features identified from the SEM micrographs. Fig. 4.3 and Fig. 4.4 show the SEM images of the degassed and gassed NBR/GO membranes, respectively, under different powers of magnification.

In Fig. 4.3 (a), it is remarked that the degassed NBR/GO membrane is covered with a network of folds on the membrane surface. The folds are arranged in a consistent orientation all over the surface as illustrated in Fig. 4.3 (b). Mensah et al. (2014) explain that the structure is attributable to the scrolling and folding effect of the GO sheet edges in the NBR matrix upon casting. When the 2D membrane structure becomes thermodynamically stable via bending, the intrinsic nature of graphene nanosheets that tends to corrugate and scroll the membrane will bring about such structure. As a result, the folds create ridges and grooves which allow effective surface area for filtration of oily wastewater. Thereby, an enhanced performance in terms of permeation flux is expected.

Upon magnification of 4000×, the folded structure of degassed NBR/GO membrane is demonstrated clearly in Fig. 4.3 (c). The grooves between the ridges are indicated with different values of width ranging from 0.411 to 1.16 μm. These observations give a mean groove width of 0.721 μm. As reported in subsection 3.6.2, the oil droplet size of the synthetic oily wastewater ranges from 1 to 50 μm and the mode size is 7 μm. The broad distribution of oil droplet size suggests that only a small quantity of oil droplets of approximately 1 μm in size will deposit in the grooves of the membrane. Since most of the oil droplets are larger in size than the groove width, they are not likely to recess and clog the membrane.

The pore size signifies the oil rejection efficiency that can be attained by a membrane. Fig. 4.3 (d) shows the pore size of 0.294 μm of the degassed NBR/GO membrane. The pores of the membrane are completely undersized on the condition

that the oil droplet diameters are of 1 μm and above. Therefore, it is presumed that the membrane is able to retain all of the oil droplets inside the synthetic oily wastewater. Apart from the enhanced permeation flux, high oil rejection efficiency is also achievable by the membrane. As the entrapped air is surfaced and removed from the latex upon degasification, large pores are developed across the membrane cross section. The fading memory effect of polymer suggests that the large pores tend to remain in shape because the entrapped air is held for some time before the elastic recoil (Malkin and Isayev, 2012). Thus, the pore size is larger as compared with the gassed NBR/GO membrane.

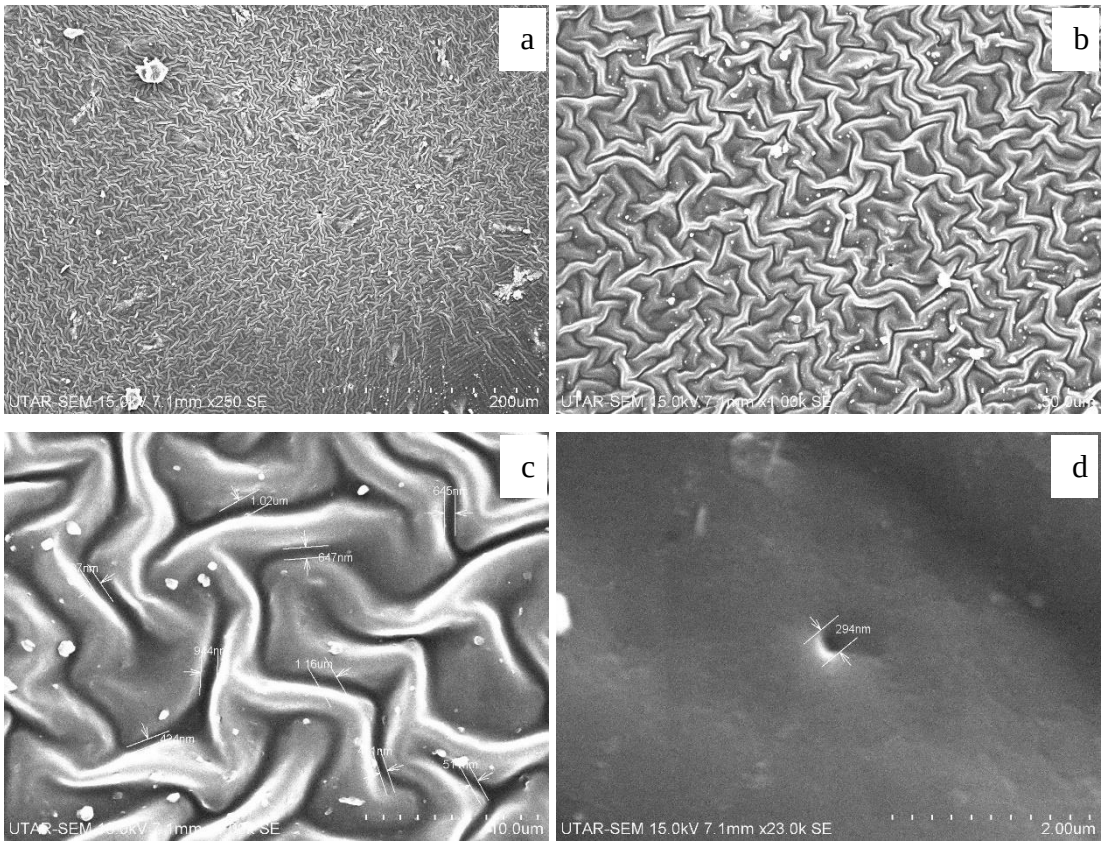


**Fig. 4.3. SEM Micrographs of Degassed NBR/GO Membrane at Magnification of (a) 250×, (b) 1000×, (c) 4000× and (d) 23000×.**

The folded structure and GO dispersion on the gassed NBR/GO membrane displayed in Fig. 4.4 (b) is similar to that of the degassed NBR/GO membrane. The ridges and grooves are formed by the regularly oriented folds, rendering effective surface area for filtration of oily wastewater. Hence, high permeation flux is expected.

The membrane surface is magnified to a power of 5000× to study the folds. Fig. 4.4 (c) is labelled with different values of width ranging from 0.483 to 1.20 µm. Relatively, the mean groove width of the gassed NBR/GO membrane (0.854 µm) is larger than that of the degassed NBR/GO membrane (0.721 µm). It thereby implies a higher tendency to membrane fouling as compared with the degassed NBR/GO membrane. However, the likeliness to clog the membrane is still very low because most oil droplets remain larger in size (1–50 µm) than the groove width.

Fig. 4.4 (d) depicts the average pore size of 0.153 µm for the gassed NBR/GO membrane. The pore size of the gassed NBR/GO membrane is relatively small by comparison with that of the degassed NBR/GO membrane (0.294 µm). Thus, it is deduced that the gassed NBR/GO membrane can offer higher oil rejection efficiency.

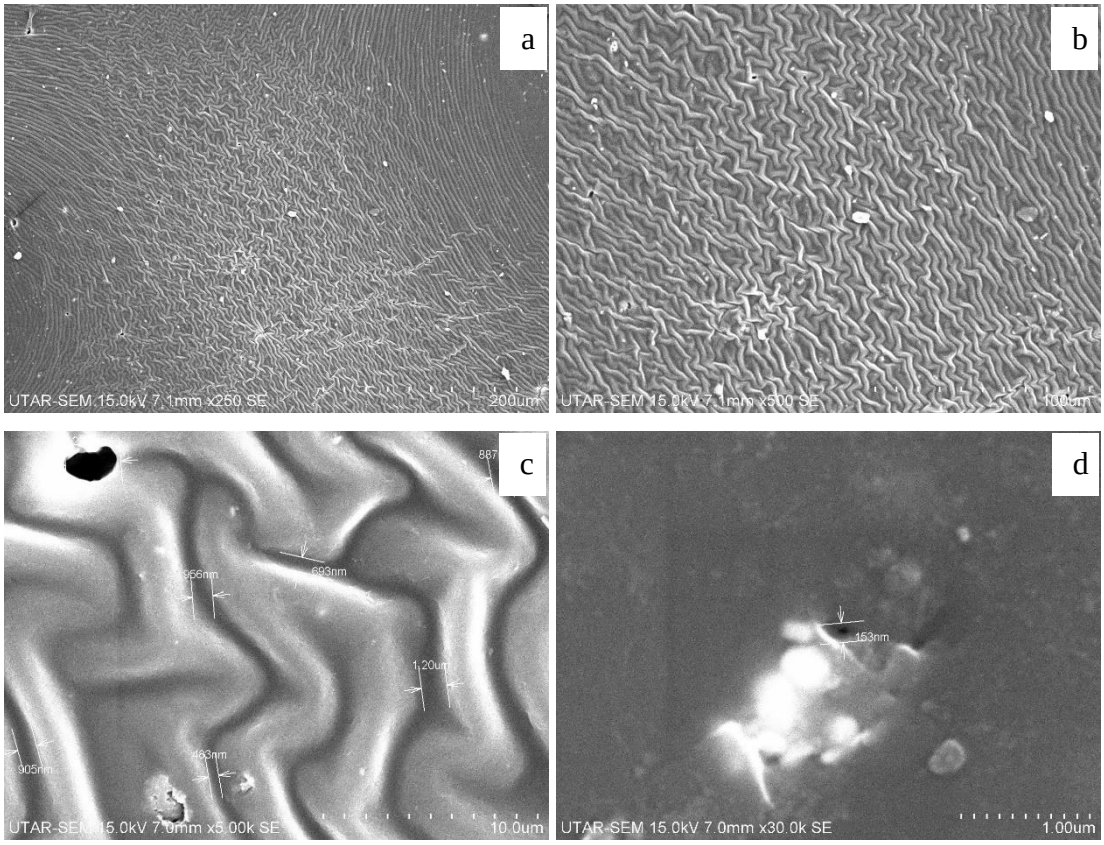


**Fig. 4.4. SEM Micrographs of Gassed NBR/GO Membrane at Magnification of (a) 250×, (b) 500×, (c) 5000× and (d) 30000×.**

### 4.2.2 AFM Analysis

AFM is designed to characterise the surface roughness of both degassed and gassed NBR/GO membranes. Different from FESEM, AFM can display average roughness ($R_a$) with the associated root-mean-square roughness ($R_q$) which are the two decisive parameters accounted to quantify membrane surface roughness. Fig. 4.5 and Fig. 4.6 present the AFM images of the degassed and gassed NBR/GO membranes, respectively. Statistics about on surface profiles of both membranes are also listed in the figures.

Fig. 4.5 (a) depicts the 2D scan of the degassed NBR/GO membrane. Apparently, the membrane surface is full of folds. Two lines are created and indicated with red and green colours in order to retrieve reasonable information of line profiles from the sample. As displayed on the line profile panel, the cross-sectional height profile of the image along the line of interest confirms that the surface is covered with ‘mountainous peaks’. The result corresponds exactly to the visual inspection of the SEM images as discussed in subsection 4.2.1.

Fig. 4.5 (a) also shows the statistics table of the line profile. The red line is drawn across a smooth region. Comparatively, the green line is selected across the dark region which represents the pore which is exceptionally large in size. Along the red and green lines, the values of peak-to-valley roughness ($R_{pv}$) are 218.923 and 471.209 nm; the values of root-mean-square roughness ($R_q$) are 40.630 and 109.854 nm; the values of average roughness ($R_a$) are 33.424 and 92.962 nm. The statistics suggest that the surface along the green line is considerably rougher due to the large pore. Therefore, it is concluded that the presence of large pores can promote the surface roughness of the degassed NBR/GO membrane to a greater extent.

The surface features of the degassed NBR/GO membrane are projected clearly on the 3D scan as shown in Fig. 4.5 (b). For instance, it is apparent that the folds have spread all over the membrane. The dark, sunken region also makes the large pore distinguishable from its surrounding. As elucidated by Huang, Ras and Tian (2018), these surface features provide effective surface area that can facilitate polar

interactions between the hydrophilic surface and water droplets, and therefore, high flux of oily wastewater filtration is achieved.

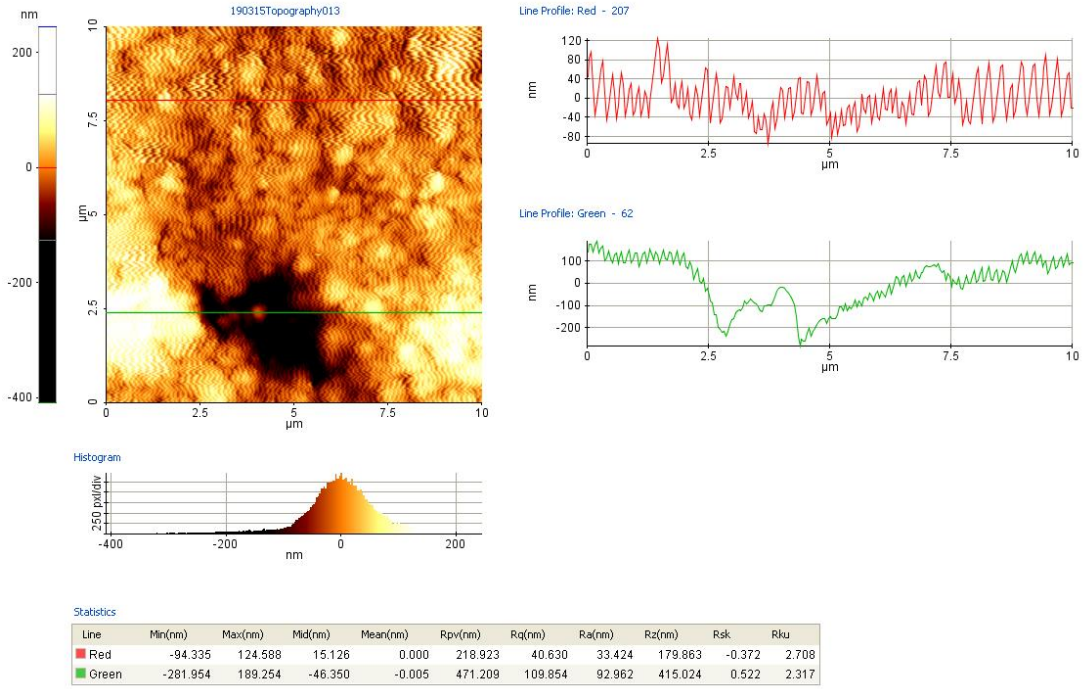


**(a)**

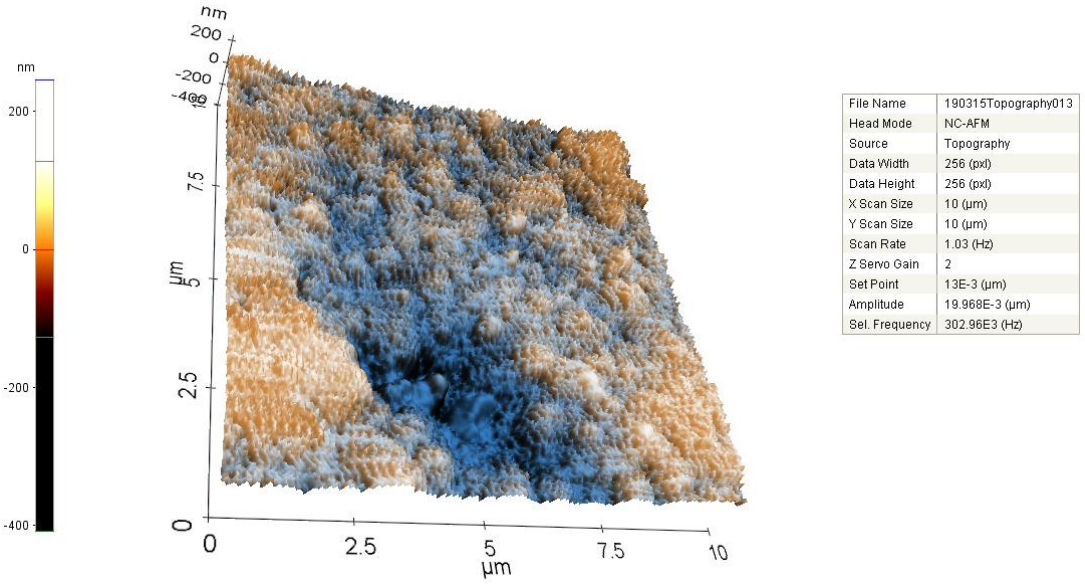


**(b)**

**Fig. 4.5. AFM Micrographs of 10 µm × 10 µm Degassed NBR/GO Membrane in (a) 2D and (b) 3D.**

The 2D scan of the gassed NBR/GO membrane is shown in Fig. 4.6 (a). The cross-sectional height profile of the image along the line of interest also justifies the folded surface of the membrane. However, the black dots which represent the pores are relatively small and uniform in size as compared with the pore size of the degassed NBR/GO membrane. The statistics table of the line profile shows that both red and green lines are almost similar with respect to $R_{pv}$, $R_q$ and $R_a$. The difference in roughness is visualised in Table 4.2 by comparing the line profile statistics of the gassed NBR/GO membrane with those of the degassed NBR/GO membrane.

**Table 4.2. Comparison of Surface Roughness between the Line Profiles of Degassed and Gassed NBR/GO Membranes.**

| Roughness (nm) | Degassed NBR/GO membrane | | Gassed NBR/GO membrane | |
|---|---|---|---|---|
| | Red | Green | Red | Green |
| $R_{pv}$ | 218.923 | 471.209 | 185.560 | 149.396 |
| $R_q$ | 40.630 | 109.854 | 31.059 | 29.794 |
| $R_a$ | 33.424 | 92.962 | 24.512 | 24.253 |

Table 4.2 suggests that the degassed NBR/GO membrane is rougher than the gassed NBR/GO membrane based on the greater values of $R_{pv}$, $R_q$ and $R_a$. It is in agreement with Fig. 4.6 (b) because less variation in the colours of the 3D surface also indicates a smoother surface. Unlike the degassed NBR/GO membrane which demonstrates large pore size, the surface of the gassed NBR/GO membrane is constituted of small pores that are uniform in size. This reduces the surface roughness of the gassed NBR/GO membrane.

The gassed NBR/GO membrane with smaller pore size can retain more oil droplets on the membrane surface. The deposited layer of oil induces additional resistance to water flux. Consequently, water flux through the gassed NBR/GO membrane is lower. The results in subsection 4.3.2 show that the gassed NBR/GO membrane, even with effective surface area for filtration, allows lower permeation fluxes at all pressures. Therefore, it is deduced that pore size remains as the dominating factor that controls the water permeability of a membrane.

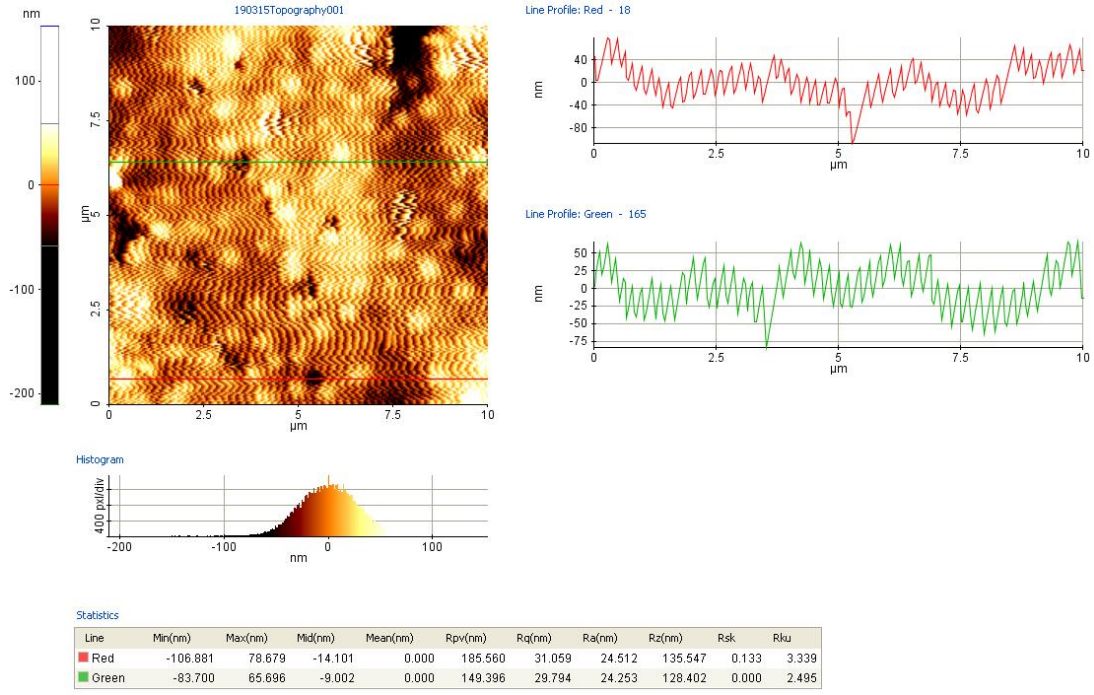


| Line | Min(nm) | Max(nm) | Mid(nm) | Mean(nm) | Rpv(nm) | Rq(nm) | Ra(nm) | Rz(nm) | Rsk | Rku |
|---|---|---|---|---|---|---|---|---|---|---|
| Red | -106.881 | 78.679 | -14.101 | 0.000 | 185.560 | 31.059 | 24.512 | 135.547 | 0.133 | 3.339 |
| Green | -83.700 | 65.696 | -9.002 | 0.000 | 149.396 | 29.794 | 24.253 | 128.402 | 0.000 | 2.495 |

**(a)**

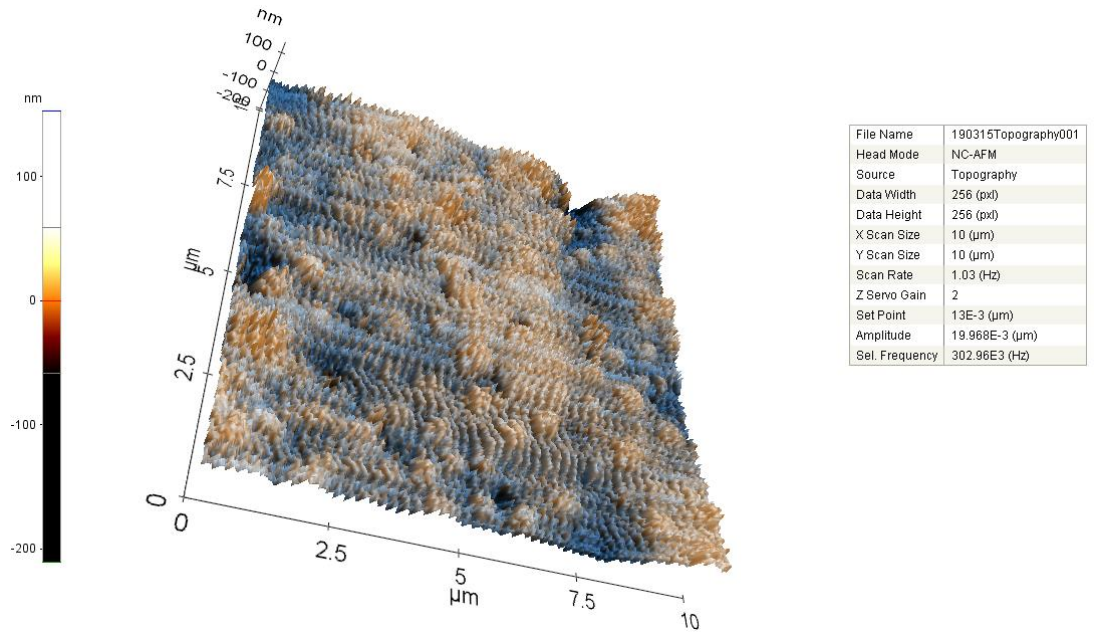

| | |
|---|---|
| File Name | 190315Topography001 |
| Head Mode | NC-AFM |
| Source | Topography |
| Data Width | 256 (pxl) |
| Data Height | 256 (pxl) |
| X Scan Size | 10 (µm) |
| Y Scan Size | 10 (µm) |
| Scan Rate | 1.03 (Hz) |
| Z Servo Gain | 2 |
| Set Point | 13E-3 (µm) |
| Amplitude | 19.968E-3 (µm) |
| Sel. Frequency | 302.96E3 (Hz) |

**(b)**

**Fig. 4.6. AFM Micrographs of 10 µm × 10 µm Gassed NBR/GO Membrane in (a) 2D and (b) 3D.**

## 4.3 Performance Tests

### 4.3.1 Tensile Properties of the Membranes

Tensile test measures the force required to break a specimen and the extent to which the specimen stretches or elongates to that breaking point. The force-strain curves as shown in Fig. 4.7 are generated by the light-weight tensile tester. Both gassed and degassed membranes exhibit similar deformation pattern before failure when subjected to tension.

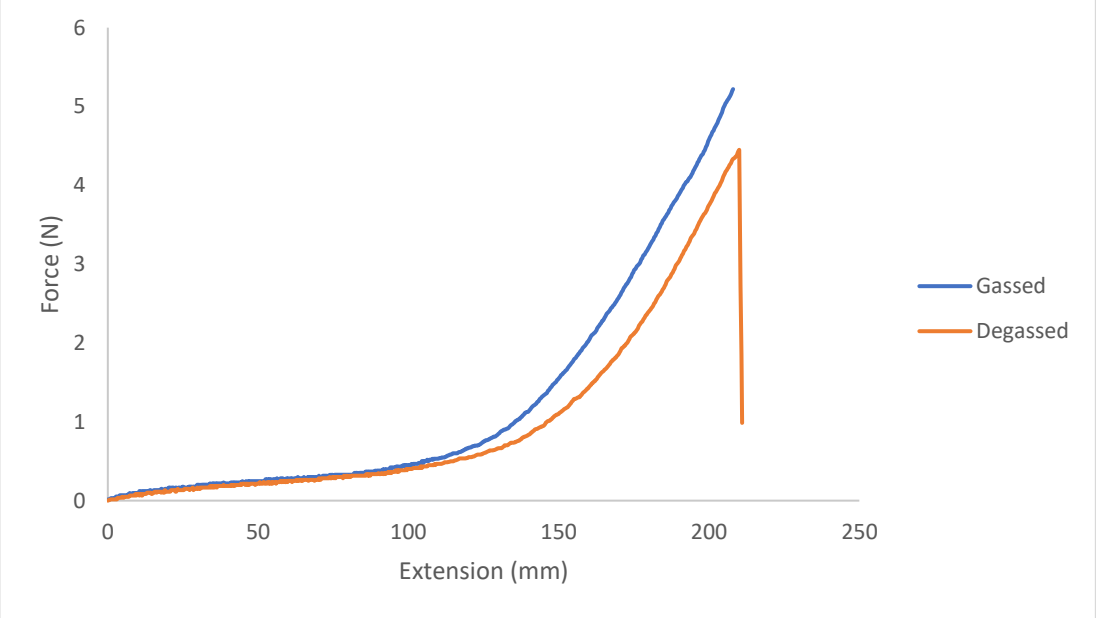


**Fig. 4.7. Force-Strain Curves of Degassed NBR/GO Membrane and Gassed NBR/GO Membrane.**

Fig. 4.8, Fig. 4.9 and Fig. 4.10 are the graphical representations of E-Modulus, ultimate tensile strength (UTS) and elongation at break that are derived from the load-strain curves. In comparison with the gassed NBR/GO membrane, the degassed NBR/GO membrane presents inferior E-Modulus and UTS of 0.503 MPa and 18.09 MPa, respectively. The presence of large pores can cause ineffective interactions between NBR chains and GO sheets. A large number of NBR chains are not anchored to the active sites on the GO surface, leaving unestablished electron donor–acceptor interaction between the nitrile groups of NBR chains and the hydroxyl groups of GO

sheets (Perez et al., 2009). The large pores limit the formation of strong interface for efficient load transfer from NBR matrix to GO, and thus, lower E-Modulus and UTS are resulted. However, the unanchored chains of the degassed NBR/GO membrane give rise to 812% of elongation at break which is greater because they are not restricted to move and align in the direction of deformation when applied with external force.

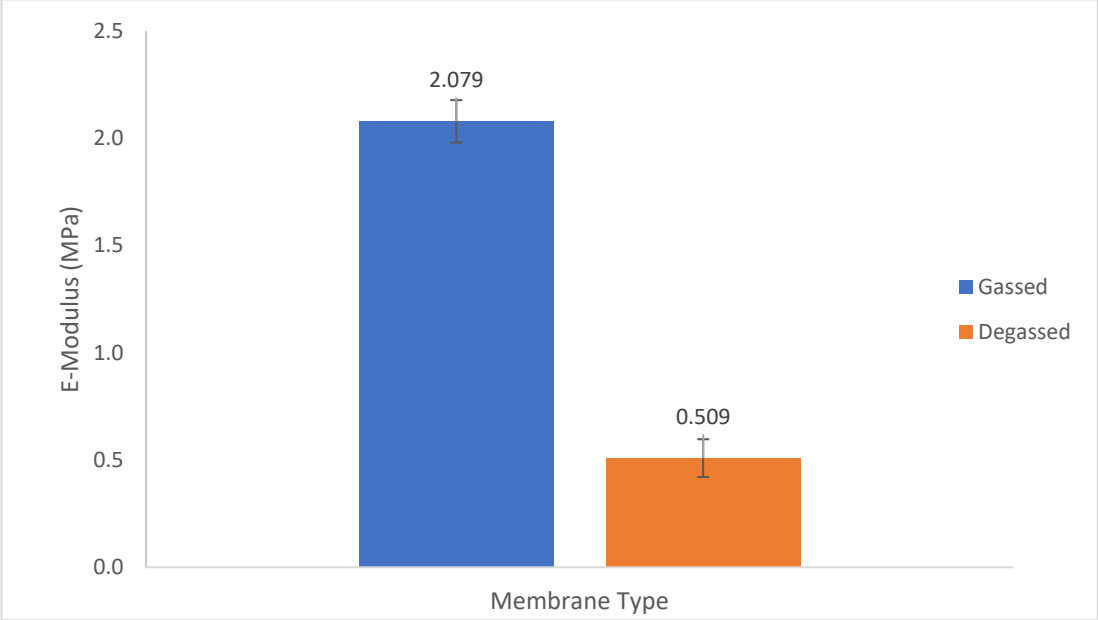


**Fig. 4.8. E-Moduli of Degassed NBR/GO Membrane and Gassed NBR/GO Membrane.**

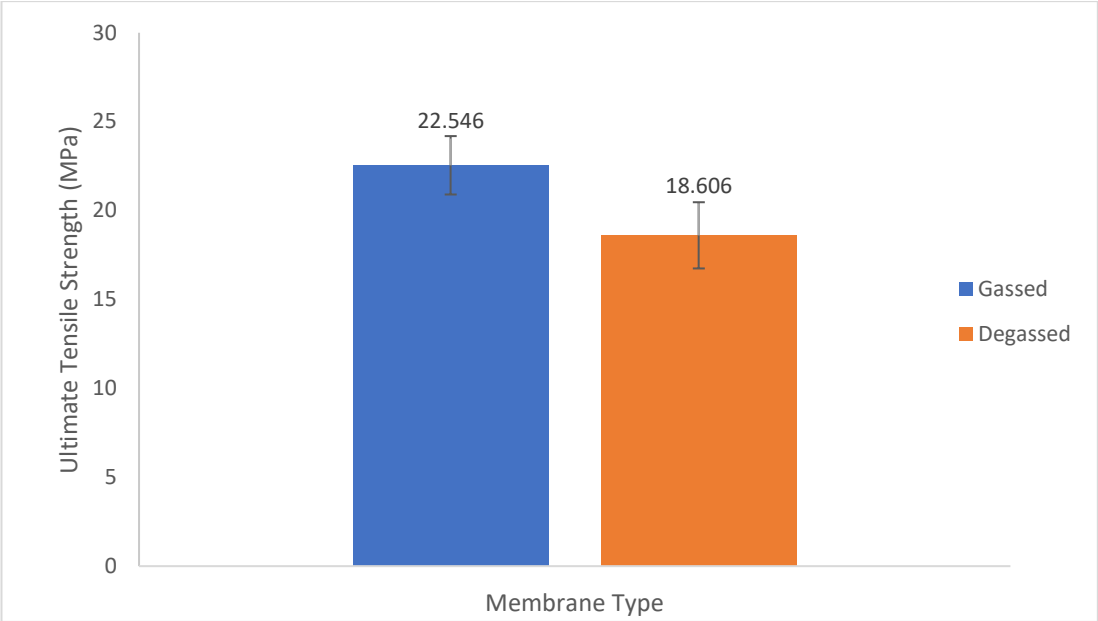


**Fig. 4.9. Ultimate Tensile Strengths of Degassed NBR/GO Membrane and Gassed NBR/GO Membrane.**

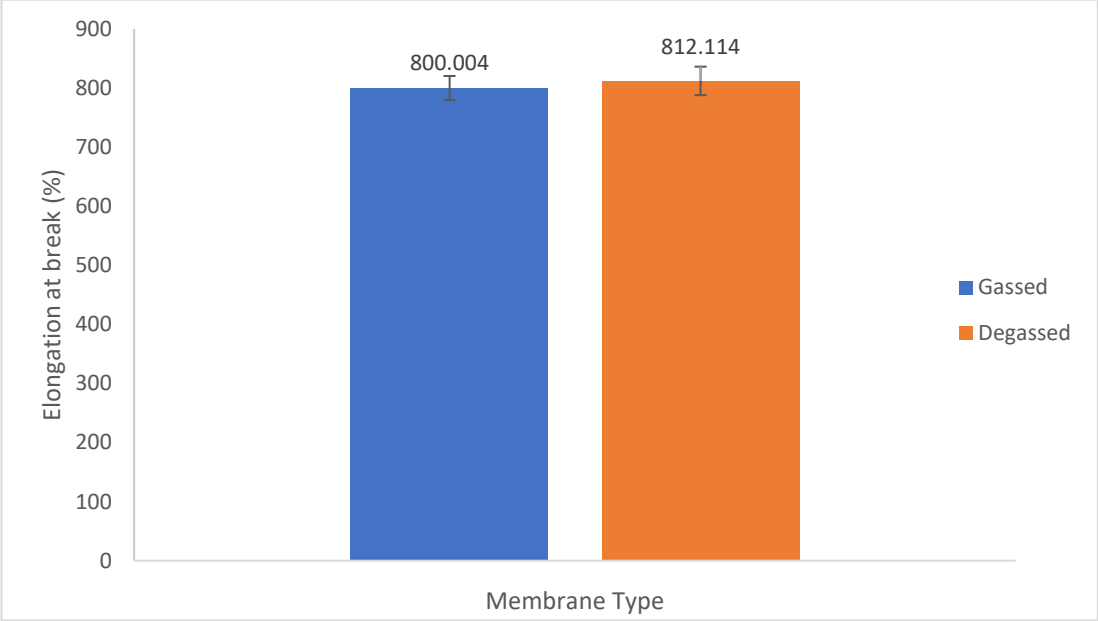


**Fig. 4.10. Elongations at Break of Degassed NBR/GO Membrane and Gassed NBR/GO Membrane.**

### 4.3.2 Permeation Flux Test for Synthetic Oily Wastewater

The degassing effect of latex-based membrane on oily wastewater filtration is also manifested by running the permeation flux test for synthetic oily wastewater. It plays a decisive part in the feasibility of a membrane because a higher rate of water flux generation is always a challenge for membrane filtration. The test was conducted whereby the time taken for a membrane to collect 30 mL of filtrate was recorded under different pressures at ambient temperature. To analyse the degassing effect, the water flux generated from the degassed NBR/GO membrane is compared with that from the gassed NBR/GO membrane in Fig. 4.11.

Fig. 4.11 (a) presents the water flux profile of membranes as a function of operating pressure when subjected to synthetic oily wastewater with diesel oil content of 1000 ppm. During the test, it was found that the degassed NBR/GO membrane was not able to withstand pressures above 0.3 bar. It broke instantly at pressures above 0.3 bar, and the wastewater was ejected without undergoing filtration. This phenomenon can be explained by the inferior UTS of the degassed NBR/GO membrane as discussed in subsection 4.3.1.

Water flux is measured at different pressures in order to show the function of operating pressure. Remarkably, water flux increases with operating pressure regardless the degassed or gassed NBR/GO membrane. When subjected to the wastewater of 1000 ppm diesel oil, the degassed NBR/GO membrane can attain the highest water flux of 2720.5332 $L/m^2 \cdot hr$ at 0.3 bar. At higher pressures, water droplets are able to pass through the membrane more readily (Gorouhi, Sadrzadeh and Mohammadi, 2006). Thereby, permeate flux and water content in permeate is higher.

Similar trends are also presented in Fig. 4.11 (b). However, water flux is slightly higher for filtration of synthetic oily wastewater with lower concentration of diesel oil. The degassed NBR/GO membrane can attain the highest water flux of 3031.4513 $L/m^2 \cdot hr$ at 0.3 bar when subjected to the wastewater with diesel oil content of 500 ppm. As compared with the oil concentration of 1000 ppm, the oil droplet size and the density increase because the concentration of oil is higher (Monash and Pugazhenthi, 2011). Coalescence of oil droplets facilitates the formation of larger

droplet size, so the coalesced oil tends to adhere on the membrane surface and cause fouling. For this reason, higher concentrations of oil will decline permeation fluxes. Consequently, both membranes demonstrate lower water fluxes at all pressures for filtration of wastewater with diesel oil content of 1000 ppm.

As compared with the gassed NBR/GO membrane, the degassed NBR/GO membrane exhibits higher water fluxes at all pressures and concentrations of diesel oil. The results are in good agreement with the surface morphology elucidating that the degassed NBR/GO membrane is characterised with larger pore size. In short, permeate flux of a membrane can be improved by increasing membrane pore size as of the degassed NBR/GO membrane, increasing operating pressure and reducing oil concentration of wastewater, along with GO that imparts hydrophilicity to the membrane surface.

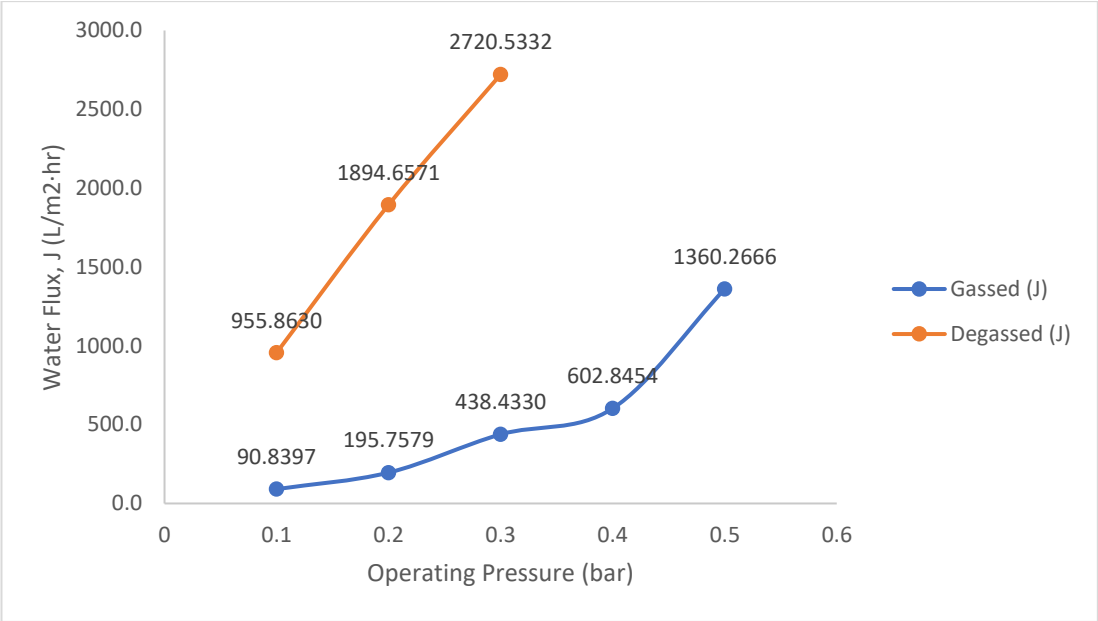


**(a)**

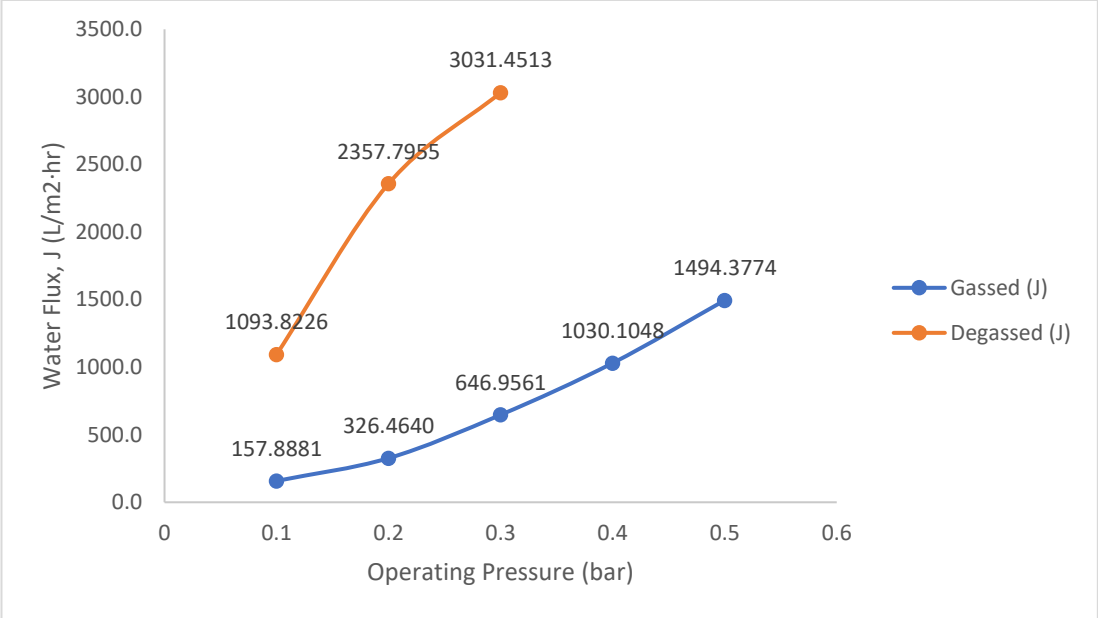


**(b)**

**Fig. 4.11. Water Flux Profile of Membranes at Different Degassing Conditions as a Function of Operating Pressure when Subjected to Synthetic Oily Wastewater with Diesel Oil Content of (a) 1000 ppm, (b) 500 ppm.**

### 4.3.3 Chemical Oxygen Demand (COD) Test

Along with the permeation flux test, the filtrate is collected for subsequent COD test so as to quantify the oil rejection efficiency attainable by each membrane. The COD levels of synthetic oily wastewaters with diesel oil contents of 1000 and 500 ppm were determined to be 5750 mg/L and 2980 mg/L, respectively. Upon the application of Eq. 3.4, the oil rejection efficiency in terms of COD removal of wastewater as a function of operating pressure is calculated and presented in Fig. 4.12. It is noted that the surfactant, SDS has also contributed to the COD levels of wastewaters and filtrates apart from the diesel oil.

Oil rejection efficiency and permeation flux show a situational decision that involves gain in the aspect of one quantity in return for diminishing another quality. The most significant observation from Fig. 4.12 is that the oil rejection efficiency is reduced whenever the water flux is enhanced. In contrast to the water flux profile as a function of operating pressure, Fig. 4.12 (a) manifests declining oil rejection efficiency when the operating pressure is increased for both membranes. Suresh et al. (2016) suggest that higher pressures promote the forced convention of wastewater across the membrane of study. The enhancement of wetting and coalescence of oil droplets is facilitated this way, and thus, oil droplets are more likely to elapse through the pores of the membrane into the permeate. As a result, the oil rejection efficiency is poor at higher pressures.

When the membranes are subjected to a lower concentration of diesel oil, the oil rejection efficiencies are slightly lower at all pressures as depicted in Fig. 4.12 (b). Suresh et al. (2016) suggests that the oil droplet size and the density reduce at low concentrations of oil. The mechanism is similar to that discussed in subsection 4.3.2. Thereby, a larger number of oil droplets can escape into the permeate because more undersized oil droplets are generated. This is the reason for the decreased oil rejection efficiency when subjected to lower concentration of diesel oil.

Relatively, the degassed NBR/GO membrane exhibits lower oil rejection efficiencies at all pressures and concentrations of diesel oil. The results are in good agreement with the surface morphology elucidating that the degassed NBR/GO

membrane is characterised with larger pore size. To conclude, oil rejection efficiency of a membrane can be improved by reducing membrane pore size as of the gassed NBR/GO membrane, reducing operating pressure and increasing oil concentration of wastewater, along with the hydrophobic nature of rubber.

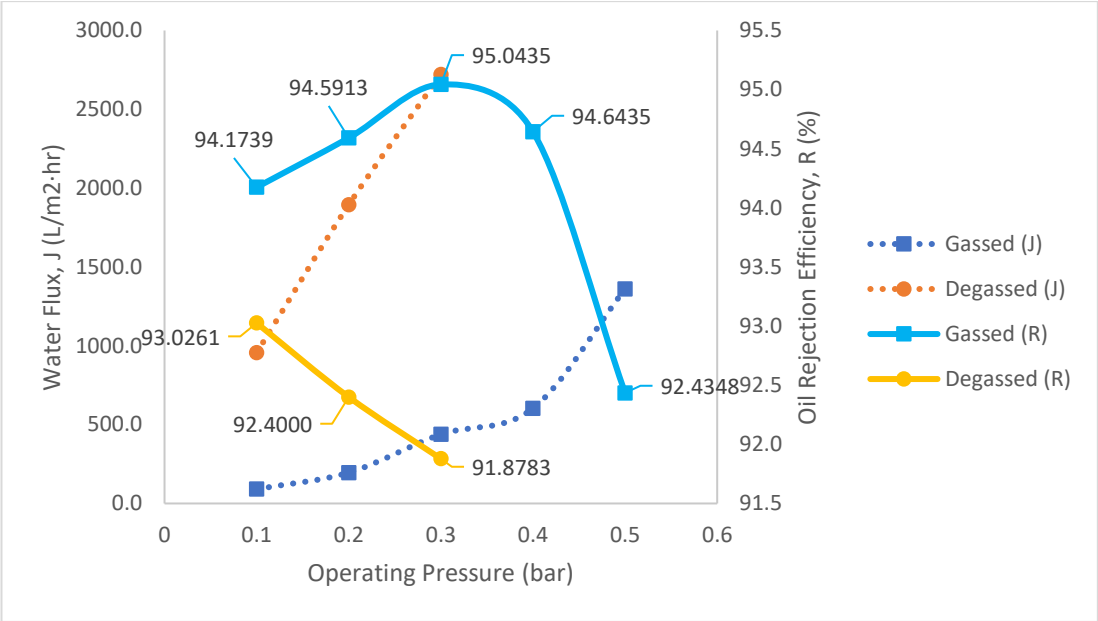


**(a)**

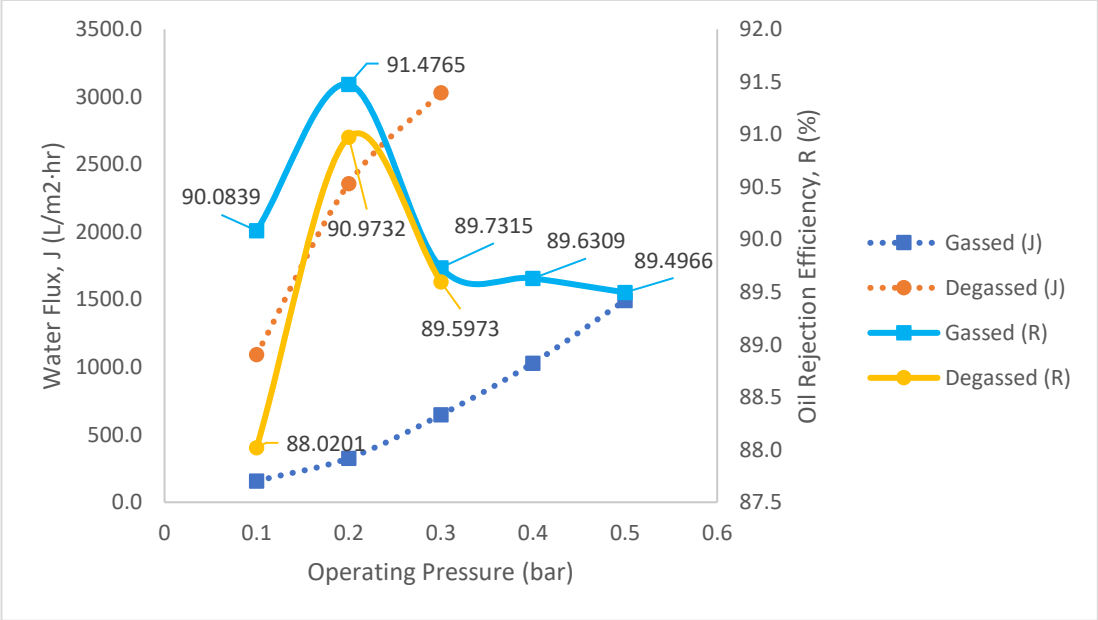


**(b)**

**Fig. 4.12. Oil Rejection Efficiency Profile of Membranes at Different Degassing Conditions as a Function of Operating Pressure when Subjected to Synthetic Oily Wastewater with Diesel Oil Content of (a) 1000 ppm, (b) 500 ppm.**

# CHAPTER 5

# CONCLUSION AND RECOMMENDATIONS

## 5.1 Conclusion

Two types of NBR/GO membrane had been successfully fabricated through latex compounding and curing method. In order to study the degassing effect on the performances of the membranes, one of the membranes was subjected to degasification by a vacuum oven. The importance of degasification was to remove entrapped air from the latex before a membrane was casted.

FTIR and XRD were conducted to characterise the graphene oxide produced through Hummers method. FTIR analysis confirmed the functionalisation of graphene sheets with oxygen-containing groups such as hydroxyl, carbonyl, epoxide and ether groups. XRD analysis established successful intercalation of oxygenated functionalities embedded in the layers of GtO by demonstrating increased interlayer spacing from 0.3382 nm for GNF to 0.7366 nm for GtO. Thus, it was concluded that the harsh oxidation had converted GNF to GtO.

The surface morphologies of both membranes were visualised by FESEM and AFM analyses. The ridges and grooves as a result of the folds allowed effective surface area for filtration of oily wastewater. The mean groove widths of the degassed and gassed NBR/GO membranes were 0.721 and 0.854 μm, respectively. Thus, the grooves would less likely trap the oil droplets larger than 1 μm. The mean pore sizes of the degassed and gassed NBR/GO membranes were 0.294 and 0.153 μm, respectively. AFM micrographs were in good agreements with SEM micrographs with

respect to the folded structure on both membranes. Besides, the AFM micrographs also presented the surface roughness analytically. Degassed NBR/GO membrane was significantly rougher than gassed NBR/GO membrane due to the presence of large pores on the degassed NBR/GO membrane.

Tensile properties of both membranes were also evaluated. The degassed NBR/GO membrane manifested inferior E-Modulus and UTS of 0.503 and 18.09 MPa respectively because the larger pores in degassed membrane limit the formation of strong interface for efficient load transfer from NBR matrix to GO. However, it exhibited superior elongation at break of 812% because more unanchored chains were able to align in the deformation direction.

In the aspects of permeation flux and oil rejection, the gassed NBR/GO membrane was preferred because it demonstrated relatively high oil rejection efficiencies at all pressures and concentrations of diesel oil. The oil rejection efficiency above 90% was the main concern in oily wastewater treatment. The permeation flux was not greatly compromised whereby the gassed NBR/GO membrane was able to achieve more than 1300 $L/m^2 \cdot hr$. This finding was already superior to most of the membranes reported in literature. The degassed NBR/GO membrane, which was characterised with large pore size, was inferior in practice.

With the view to commercialising the membrane in oily wastewater treatment, the gassed NBR/GO membrane is able to achieve promising performances because its surface morphology suggests smaller and more uniform pore size. It is also stronger in terms of E-Modulus and UTS to withstand extreme conditions. In addition, high oil rejection efficiency is attainable without compromising too much on permeation flux.

## 5.2 Recommendations

The uncovered areas in this study had been revealed along the way when the experiment regarding to the degassing effect was conducted. Apart from the considerations in previous researches, further studies that extend to all facets of the factors governing membrane performances in filtration technology must be conducted to continually develop the membrane. They are hereby brought to recommendations because there is still room for improvement of the implemented findings from the previous researches.

The membrane performances are susceptible to latex TSC. Varying TSC of latex is to investigate whether the water content in latex would impose any significant influence on the membrane performances. There is a point whereby the TSC of latex can achieve the most promising performances of a membrane for oily wastewater filtration.

Exfoliation parameters, that might affect GO dispersion in NBR matrix, are uncertain. Ultrasonification of 30 minutes is insufficient to fully exfoliate GtO. It is a possible reason that might lead to the formation of GO agglomerates. Thus, it is recommended to extensively study the exfoliation time, the amplitude and the pulse required to completely break the layered GtO into GO sheets.

Membrane thickness also plays a decisive part in oily wastewater filtration. The fact that the membrane of study was only able to withstand low pressures indicates the insufficient strength of the 0.05 mm thick membrane. In order to achieve practical usage in heavy oil wastewater, a membrane must be strong enough against the extreme conditions. However, permeation flux will invariably decrease when the membrane thickness increases. Therefore, a study about membrane thickness to achieve balance between tensile properties and permeation flux is recommended.

Palm oil industry shares the largest portion of oily wastewater contributor in Malaysia. Instead of petroleum refinery effluent, POME is recommended for the study of interest to a wider audience. A close simulation of filtration can be carried out by feeding POME into the dead-end membrane test rig so as to analyse the membrane

performances with respect to permeation flux and oil rejection efficiency. Simultaneously, the membrane performances against other constituents in POME such as total suspended solids and total nitrogen can also be manifested.

# REFERENCES

Abadi, S. R. H., Sebzari, M. R., Hemati, M., Rekabdar, F. and Mohammadi, T., 2011. Ceramic membrane performance in microfiltration of oily wastewater. *Desalination*, 265(1–3), pp. 222–228.

Ahmad, A. L., Sumathi, S. and Hameed, B. H., 2006. Coagulation of residue oil and suspended solid in palm oil mill effluent by chitosan, alum and PAC. *Chemical Engineering Journal*, 118(1–2), pp. 99–105.

Ahmadi, M., Zoroufchi Benis, K., Faraji, M., Shakerkhatibi, M. and Aliashrafi, A., 2019. Process performance and multi-kinetic modeling of a membrane bioreactor treating actual oil refinery wastewater. *Journal of Water Process Engineering*, 28, pp. 115–122.

Aljuboury, D. A. D. A., Palaniandy, P, Abdul Aziz, H. B. and Feroz, S., 2017. Treatment of petroleum wastewater by conventional and new technologies: A review. *Global Nest Journal*, 19, pp. 1–14.

Aloui, F., Kchaou, S. and Sayadi, S., 2009. Physicochemical treatments of anionic surfactants wastewater: Effect on aerobic biodegradability. *Journal of Hazardous Materials*, 164(1), pp. 353–359.

Álvarez, L. O., 2018. *Chain dynamics in crosslinked filled and unfilled polymer blends of different miscibility*. [online] Available at: <http://cfm.ehu.es/view/files/TESIS_ORTEGA_ALVAREZ_LUCIA.pdf> [Accessed 14th March 2018].

Ameta, S. and Ameta, R., 2018. *Advanced Oxidation Processes for Wastewater Treatment*. 1st ed. India: Academic Press.

Anthuvan Babu, S., Raja, S., Sibi, S. and Sundaram, T. T., 2011. *Direct and Indirect Electrochemical Oxidation of Organic Pollutants from Industrially Polluted Water*.

[online] Available at: <http://www.icontrolpollution.com/articles/direct-and-indirect-electrochemical-oxidation-of-organicpollutants-from-industrially-polluted-water-.php?aid=45692> [Accessed 22nd June 2018].

Asatekin, A. and Mayes, A. M., 2009. Oil industry wastewater treatment with fouling resistant membranes containing amphiphilic comb copolymer. *Environmental Science Technology*, 43(12), pp. 4487–4492.

Bai, X., Wan, C., Zhang, Y. and Zhai, Y., 2011. Reinforcement of hydrogenated carboxylated nitrile–butadiene rubber with exfoliated graphene oxide. *Carbon*, 49(5), pp. 1608–1613.

Brandt, M. J., Johnson, K. M., Elphinston, A. J. and Ratnayaka, D. D., 2017. Storage, Clarification and Chemical Treatment. *Twort's Water Supply*, pp. 323–366.

Caltest Analytical Laboratory, 2014. *Oil & Grease Analyses*. [online] Available at: <https://www.caltestlabs.com/Services/OilGreaseAnalyses.aspx> [Accessed 5th January 2019].

Coran, A. Y., 2013. Vulcanization. *The Science and Technology of Rubber*, pp. 337–381.

Couto, C. F., Lange, L. C. and Amaral, M. C. S., 2018. A Critical Review on Membrane Separation Processes Applied to Remove Pharmaceutically Active Compounds from Water and Wastewater. *Journal of Water Process Engineering*, 26, pp. 156–175.

Diya'uddeen, B. H., Daud, W. M. A. W. and Abdul Aziz, A. R., 2011. Treatment technologies for petroleum refinery effluents: A review. *Process Safety and Environmental Protection*, 89(2), pp. 95–105.

El-hoshoudy, A. N. M. B., 2018. Emulsion Polymerization Mechanism. *Recent Research in Polymerization*, 1, pp. 3–14.

Etchepare, R., Oliveira, H., Azevedo, A. and Rubio, J., 2017. Separation of emulsified crude oil in saline water by dissolved air flotation with micro and nanobubbles. *Separation and Purification Technology*, 186, pp. 326–332.

Gorouhi, E., Sadrzadeh, M. and Mohammadi, T., 2006. Microfiltration of oily wastewater using PP hydrophobic membrane. *Desalination*, 200(1-3), pp. 319–321.

Gupta, A. and Yan, D., 2016. *Mineral Processing Design and Operations: An Introduction*. 2nd ed. Oxford: Elsevier Science Ltd.

Hanhi, K., Poikelispää, M. and Tirilä, H. M., 2007. *Elastomeric materials*. Finland: Tampere University of Technology, The Laboratory of Plastics and Elastomer Technology.

Huang, S., Ras, R. H. A. and Tian, X., 2018. Antifouling membranes for oily wastewater treatment: Interplay between wetting and membrane fouling. *Current Opinion in Colloid & Interface Science*, 36, pp. 90–109.

International Trade Administration, 2016. *2016 ITA Environmental Technologies Top Markets Report.* [online] Available at: <https://www.trade.gov/topmarkets/pdf/Environmental_Technologies_Southeast_Asia.pdf> [Accessed 2nd April 2019].

Ionita, M., Pandele, A. M., Crica, L. and Pilan, L., 2014. Improving the thermal and mechanical properties of polysulfone by incorporation of graphene oxide. *Composites: Part B*, 59, pp. 133–139.

Ishak, S. and Malakahmad, A., 2013. Optimization of Fenton process for refinery wastewater biodegradability augmentation. *Korean Journal of Chemical Engineering*, 30(5), pp. 1083–1090.

Jiang, Y., Wang, W. N., Liu, D., Nie, Y., Li, W., Wu, J., Zhang, F., Biswas, P. and Fortner, J. D., 2015. Engineered Crumpled Graphene Oxide Nanocomposite Membrane Assemblies for Advanced Water Treatment Processes. *Environmental Science & Technology*, 49(11), pp. 6846–6854.

Joseph, R., 2013. *Practical Guide to Latex Technology*. 1st ed. Shawbury: Smithers Rapra.

JWC Environmental, 2019. What is a DAF? [online] Available at: <https://www.jwce.com/knowledge-center/what-is-a-daf/> [Accessed 7th April 2019].

Koay, E., 2018. *Latex-Based Membrane for Oily Wastewater Filtration: Study on the Sulfur Concentration Effect*.

Li, Q. X., Kang, C. B. and Zhang, C. K., 2005. Waste Water Produced from an Oilfield and Continuous Treatment with an Oil-Degrading Bacterium. *Process Biochemistry*, 40(2), pp. 873–877.

Li, Y. J., Wang, F., Zhou, G. D. and Ni, Y. M., 2003. Aniline Degradation by Electrocatalytic Oxidation. *Chemosphere*, 53(10), pp. 1229–1234.

Liu, G. H., Ye, Z. F., Tong, K. and Zhang, Y. H., 2013. Biotreatment of heavy oil wastewater by combined upflow anaerobic sludge blanket and immobilized biological aerated filter in a pilot-scale test. *Biochemical Engineering Journal*, 72, pp. 48–53.

Malas, A., 2017. Rubber nanocomposites with graphene as the nanofiller. *Progress in Rubber Nanocomposites*, pp. 179–229.

Malaysia Palm Oil Council, 2012. *Malaysian Palm Oil Industry*. [online] Available at: <http://www.mpoc.org.my/Malaysian_Palm_Oil_Industry.aspx> [Accessed 20th June 2018].

Malkin, A. Y. and Isayev, A. I., 2012. Viscoelasticity. *Rheology: Concepts, Methods, and Applications*. 2nd ed. Toronto: ChemTec Publishing.

MDA Filtration Inc, 2013. *Filtration Spectrum*. [online] Available at: <http://www.mdafiltration.com/filtration-spectrum.html> [Accessed 7th April 2019].

Mensah, B., Kim, S. J., Arepalli, S. and Nah, C. W., 2014. A Study of Graphene Oxide-Reinforced Rubber Nanocomposite. *Journal of Applied Polymer Science*, 131(16), pp. 1–9.

Mittal, P., Jana, S. and Mohanty, K., 2011. Synthesis of low-cost hydrophilic ceramic–polymeric composite membrane for treatment of oily wastewater. *Desalination*, 282, pp. 54–62.

Monash, P. and Pugazhenthi, G., 2011. Effect of TiO2 addition on the fabrication of ceramic membrane supports: A study on the separation of oil droplets and bovine serum albumin (BSA) from its solution. *Desalination*, 279(1-3), pp. 104–114.

Painmanakul, P., Sastaravet, P., Lersjintanakarn, S. and Khaodhiar, S., 2010. Effect of bubble hydrodynamic and chemical dosage on treatment of oily wastewater by

Induced Air Flotation (IAF) process. *Chemical Engineering Research and Design*, 88(5–6), pp. 693–702.

Paredes, J. I., Villar-Rodil, S., Martínez-Alonso, A. and Tascón, J. M. D., 2008. Graphene Oxide Dispersions in Organic Solvents. *Langmuir*, 24(19), pp. 10560–10564.

Perez, L. D., Zuluaga, M. A., Kyu, T., Mark, J. E. and Lopez, B. L., 2009. Preparation, characterization, and physical properties of multiwall carbon nanotube/elastomer composites. *Polymer Engineering & Science*, 49(5), pp. 866–874.

Qureshi, T. S. and Panesar, D. K., 2019. Impact of graphene oxide and highly reduced graphene oxide on cement based composites. *Construction and Building Materials*, 206, pp. 71–83.

Saber, A., Hasheminejad, H., Taebi, A. and Ghaffari, G., 2013. Optimization of Fenton-based treatment of petroleum refinery wastewater with scrap iron using response surface methodology. *Applied Water Science*, 4(3), pp. 283–290.

Salahi, A., Noshadi, I., Badrnezhad, R., Kanjilal, B. and Mohammadi, T., 2013. Nano-porous membrane process for oily wastewater treatment: Optimization using response surface methodology. *Journal of Environmental Chemical Engineering*, 1(3), pp. 218–225.

Santander, M., Rodrigues, R. T. and Rubio, J., 2011. Modified jet flotation in oil (petroleum) emulsion/water separations. *Colloids and Surfaces A: Physicochemical and Engineering Aspects*, 375(1-3), pp. 237–244.

Sarfaraz, M. V., Ahmadpour, E., Salahi, A., Rekabdar, F. and Mirza, B., 2012. Experimental investigation and modelling hybrid nano-porous membrane process for industrial oily wastewater treatment. *Chemical Engineering Research and Design*, 90(10), pp. 1642–1651.

Singh, R. K., Kumar, R. and Singh, D. P., 2016. Graphene oxide: strategies for synthesis, reduction and frontier applications. *RSC Advances*, 6(69), pp. 64993–65011.

Song, C. W., Wang, T. H., Pan, Y. Q. and Qiu, J. S., 2006. Preparation of coal-based microfiltration carbon membrane and application in oily wastewater treatment. *Separation and Purification Technology*, 51(1), pp. 80–84.

StarThermoplastics, 2018. *Thermoplastic vs Thermoset*. [online] Available at: <https://www.starthermoplastics.com/our-chemistry/thermoplastic_vs_thermoset/> [Accessed 28th February 2019].

SUEZ Water Technologies, 2018. *Membrane vs Conventional Technology*. [online] Available at: <https://www.suezwatertechnologies.com/images/watertour/v2/pdf/events/australia/breakout/Bkout%20-%20Membrane%20vs[1].%20Conventional%20Tech%20(Bandick-LaFlamme).pdf> [Accessed 24th February 2019].

Suresh, K., Srinu, T., Ghoshal, A. K. and Pugazhenthi, G., 2016. Preparation and characterization of TiO2 and γ-Al2O3 composite membranes for the separation of oil-in-water emulsions. *RSC Advances*, 6(6), pp. 4877–4888.

Tchobanoglous, G., Stensel, D. H., Tsuchihashi, R. and Burton, F., 2014. *Wastewater Engineering: Treatment and Reuse*. 5th ed. New York: McGraw-Hill.

Ursino, C., Castro-Muñoz, R., Drioli, E., Gzara, L., Albeirutty, M. H. and Figoli, A., 2018. Progress of Nanocomposite Membranes for Water Treatment. *Membranes 2018*, 8(2), pp. 1–40.

Wang, J., Li, S. Y., Jiang, F., Wu, K., Liu, G. L., Lu, H. and Chen, G. H., 2015. A Modified Oxic-Settling-Anaerobic Activated Sludge Process Using Gravity Thickening for Excess Sludge Reduction. *Scientific Reports*, 5(1), pp. 1–10.

Wu, L., Ge, G. and Wan, J. B., 2009. Biodegradation of oil wastewater by free and immobilised Yarrowia lipolytica W29. *Journal of Environmental Sciences*, 21(2), pp. 237–242.

Xia, S. J., Yao, L. J., Zhao, Y., Li, N. N. and Zheng, Y., 2015. Preparation of graphene oxide modified polyamide thin film composite membranes with improved hydrophilicity for natural organic matter removal. *Chemical Engineering Journal*, 280, pp. 720–727.

Xu, Z. W., Zhang, J. G., Shan, M. J., Li, Y. L., Li, B. D., Niu, J. R., Zhou, B. M. and Qian, X.M., 2014. Organosilane-functionalized graphene oxide for enhanced antifouling and mechanical properties of polyvinylidene fluoride ultrafiltration membranes. *Journal of Membrane Science*, 458, pp. 1–13.

Yang, T., Ma, Z. F. and Yang, Q. Y., 2011. Formation and performance of Kaolin/MnO2 bi-layer composite dynamic membrane for oily wastewater treatment: Effect of solution conditions. *Desalination*, 270(1–3), pp. 50–56.

Yargeau, V., 2012. *Metropolitan Sustainability: Understanding and Improving the Urban Environment*. 1st ed. Cambridge: Woodhead Publishing Limited.

Yu, L., Han, M. and He, F., 2017. A review of treating oily wastewater. *Arabian Journal of Chemistry*, 10, pp. 1913–1922.

Yu, S. L., Lu, Y. N., Chai, B. X. and Liu, J. H., 2006. Treatment of oily wastewater by organic–inorganic composite tubular ultrafiltration (UF) membranes. *Desalination*, 196(1–3), pp. 76–83.

Zavastin, D., Cretescu, I., Bezdadea, M., Bourceanu, M., Drăgan, M., Lisa, G., Mangalagiu, I., Vasić, V. and Savić, J., 2010. Preparation, characterization and applicability of cellulose acetate–polyurethane blend membrane in separation techniques. *Colloids and Surfaces A: Physicochemical Engineering Aspects*, 370(1–3), pp. 120–128.

Zeng, Y. B., Yang, C. Z., Zhang, J. D. and Pu, W. H., 2007. Feasibility investigation of oily wastewater treatment by combination of zinc and PAM in coagulation/flocculation. *Journal of Hazardous Materials*, 147(3), pp. 991–996.

Zhang, Y. Q., Cui, P., Du, T. D., Shan, L. B. and Wang, Y. L., 2009. Development of a sulfated Y-doped nonstoichiometric zirconia/polysulfone composite membrane for treatment of wastewater containing oil. *Separation and Purification Technology*, 70(2), pp. 153–159.

Zhao, X., Wang, Y. M., Ye, Z. F., Borthwick, A. and Ni, J. R., 2006. Oil field wastewater treatment in Biological Aerated Filter by immobilized microorganisms. *Process Biochemistry*, 41(7), pp. 1475–1483.

Zhao, Y. Q., 2003. Correlations between Floc Physical Properties and Optimum Polymer Dosage in Alum Sludge Conditioning and Dewatering. *Chemical Engineering Journal*, 92(1–3), pp. 227–235.